Batch and Bulk Adsorptive Removal of Anionic Dye using Metal/Halide-Free Ordered Mesoporous Carbon as Adsorbent

Jyoti Mittal[a], Asna Mariyam[a], Farzeen Sakina[b], Richard T. Baker[b*], Ashok K. Sharma[c] and Alok Mittal[a*]

a. Department of Chemistry, Maulana Azad National Institute of Technology, Bhopal 462 003, India.
b. Department of Chemistry, University of St. Andrews, St. Andrews, Fife KY16 9AJ, United Kingdom.
c. Department of Chemistry, Deenbandhu Chhotu Ram University of Science & Technology, Murthal, Sonipat 131039, India.

*Corresponding authors
Richard T. Baker: E: rtb5@st-andrews.ac.uk; T: +441334463899; F: +441334463808

Abstract

The present report is an outcome of investigations to assess the adsorptive potential of a synthesized metal- and halide-free variant of ordered mesoporous carbon (OMC) towards an anionic azo dye, Methyl Orange. The results of preliminary studies, carried out in batch mode, helped in setting up the process variables to achieve optimum adsorption conditions. The experimental data were then fitted to Langmuir, Freundlich, Temkin, and Dubinin-Radushkevitch isotherm models. The equilibrium data fitted well to the Langmuir model at 303 K and the monolayer adsorption capacity was 0.33 $mmol.g^{-1}$. The adsorption kinetics were explored by fitting the data to pseudo-first-order and pseudo-second-order kinetic models. The latter described the kinetics well, as indicated by higher regression coefficients. To elucidate the mechanism of mass transfer, various well-known mathematical models were employed. The adsorption of the dye was found to involve particle diffusion. Thermodynamic studies revealed that the adsorptive uptake of Methyl Orange by the OMC was spontaneous (ΔG^0 = -23.71 $kJ.mol^{-1}$) and exergonic (ΔH^0 = -123.15 $kJ.mol^{-1}$). Finally, the bulk removal of the anionic dye was investigated through column operations followed by column regeneration (desorption) studies. Column saturation of up to 96.55 % could be realized. Values for dye recovery, however, reached up to 93.26 %. The column efficiency was then evaluated by carrying out three consecutive adsorption/desorption cycles. The results obtained indicated that the adsorbent has a good ability to eliminate Methyl Orange from wastewater, both in batch and column operations.

Keywords: Methyl Orange, Adsorption, Isotherms, Kinetics, Particle-diffusion, Bulk Removal, Wastewater Treatment

1. Introduction

A large part of effluents from industries such as paper, textiles, pharmaceuticals, printing, leather, etc. consists of synthetic organic dyes and more than 1,00,000 different commercial dyes are used globally. These dyes are ultimately potential water contaminants if the untreated water with spent dyestuff is released into waterways (Chen et al., 2010). The contamination of water resources with dyes is of great concern for various reasons. Most dyes have been reported to be toxic (Tsuboy et al., 2007), carcinogenic (Golka et al., 2004), mutagenic (Chung, 2000), or even teratogenic (Beaudoin and Pickering, 1960). Apart from being a menace to aqueous life by blocking the penetration of sunlight into the water body and hindering photosynthesis (Jadhav et al., 2019), the dyes also decrease the aesthetic value of the water bodies due to their high visibility even when present in very small amounts (Liu et al., 2014). They are often inert to oxidation and degradation due to highly stable skeletal structures, rendering their removal problematic (Bharti et al., 2019). A wide range of methods, classified as physical methods like adsorption (Kanwal et al., 2017), coagulation-flocculation (Wong et al., 2007), ion-exchange (Hassan and Carr, 2018), etc.; chemical methods like oxidation (Nidheesh et al., 2018), ozonation (Soares et al., 2006), photocatalysis (H. Hamad et al., 2020; Sadik et al., 2019) etc.; and biological methods including algal degradation (Omar, 2008) and enzymatic degradation (Joshni and Subramaniam, 2011), have been employed in practice. To date, adsorption has been considered the most appropriate and efficient technique for the removal of dyes from wastewater due to the easy handling of the adsorbent and the fact that it gives rise to no harmful by-products (Anastopoulos et al., 2018).

An extensive range of carbon-based adsorbents, such as graphene oxide (Bhattacharya et al., 2017), carbon-nanotubes (Rajabi et al., 2017), activated carbon (Gupta and Suhas, 2009), and biochar (Mohan et al., 2006) have been used for many years as adsorbents in the treatment of dye-polluted waters. However, recently, Ordered Mesoporous Carbons (OMCs)

have generated much interest as advanced potential adsorbents in the field of dye removal (Gang et al., 2021). This is because of their novel properties which include very high specific surface area, large pore volumes, and mesoscale (few nm) pore diameters. In addition, the size and shape of their pores can be tuned by altering preparative parameters and the chemistry of their pore surfaces can also be easily modified. The ordered nature of the pore structures of OMCs is an outcome of a narrow pore-size distribution which is reported to result in superior adsorption capacities and faster adsorption rates (Gang et al., 2021; Wu and Zhao, 2011).

The main aims of this current contribution are to assess the potential of an OMC material, synthesized through an unconventional route (discussed later), to remove, by adsoption from solution, the widely-used dye, Methyl Orange (MO), to determine the kinetics and thermodynamics of the interaction of OMC with MO, and to evaluate the reversibility of the adsorption process. MO is a toxic, anionic, mono-azo dye, also known as Orange III. At room temperature, this compound appears as an orange solid and is used in analytical chemistry as an internal indicator in acid-base titrations. Its removal through conventional techniques, however, is challenging due to its high solubility in water (Akansha et al., 2019). In a study on developing rats, MO was found to influence the microbial succession and the activities of intestinal enzymes. Enzymatic activities of nitroreductase and azo reductase were significantly enhanced and resulted in the appearance of anaerobes in the large intestine (Chang et al., 1994). If ingested accidentally, reductase enzymes in the intestine and liver may catalyse the cleavage of the azo group in MO, leading to the formation of aromatic amines which are potential carcinogens and may lead to intestinal cancer (Chung, 1983; Chung et al., 1992).

2. Materials and Methods

All the chemicals used in the preparation of the OMC and during its subsequent evaluation as a dye adsorbent were of analytical grade. A detailed description of the synthesis, characterisation, and batch and continuous mode operations, is presented in this section.

2.1 Adsorbent Preparation

The synthesis of the OMC was carried out as described in a previous report by the authors (Sakina and Baker, 2019) and is summarised in the diagram in Figure 1. A two-phase technique was adopted that made use of organic-organic self-assembly of ordered micelles of a block copolymer surfactant (F127) to construct a soft template whose function was to direct the formation of the carbonaceous material during its polymerisation from resorcinol and formaldehyde precursors, such that it formed with an ordered mesoporous structure. The synthesis involved two steps: polymerisation, catalysed by ammonium hydroxide, followed by condensation that used oxalic acid as a catalyst. By deliberately using completely degradeable catalysts, rather than the mineral acids and bases conventionally used, it was hoped to develop a multifunctional OMC material - without halide or metal ion contaminants - that could be used as an adsorbent but also as a support in heterogeneous catalysis, in which such contaminants often poison and deactivate the catalyst material. In brief, the first step was initiated by allowing formaldehyde (2.26 g of 37 wt % solution in water) and resorcinol (2.20 g) to react for a period of 1 h under stirring. The ammonium hydroxide catalyst (2 mL of 0.1 M aqueous solution) was then added and the mixture was stirred for 1 h, giving rise to a solution of oligomers known as a resol. The resol was added to a solution of F127 block copolymer (1.60 g), ethanol (10 g), and water (8 g), and this mixture was stirred for 20 min before the addition of the oxalic acid condensation catalyst (0.225 g). After 5-10 min of further stirring, the solution turned from clear to cloudy as phase separation took place. The mixture was stirred for a further hour and left to stand for about 12 h to obtain the polymer

gel. This was then subjected to curing and drying at 80 °C for 24 h and was finally carbonised at 400 °C in a tube furnace (heating rate 1°C min^{-1}) under a flowing inert atmosphere (100 mL min^{-1} of N_2 at STP) for 3 h, after which the OMC product was recovered.

2.2 Material Characterization

Nitrogen gas physisorption, Small Angle (SA) XRD, Transmission Electron Microscopy (TEM), Scanning Electron Microscopy (SEM), X-ray Photoelectron Spectroscopy (XPS) and Fourier Transfer Infrared (FTIR) and Solid-state ^{13}C-NMR Spectroscopy were used to characterize the OMC material synthesized. A Micromeritics TriStar II 3020 instrument operating at liquid nitrogen temperature was used to obtain nitrogen physisorption isotherms (with samples degassed at 393 K for at least 12 h before measurement). The software supplied by the instrument manufacturer was used to retrieve the Barrett, Joyner, and Halenda (BJH) pore-size distribution data. A PANanalytical Empyrean instrument utilising Cu Kα radiation and operating in reflectance geometry was employed to obtain the SAXRD diffractogram. TEM was carried out using a JEOL 2011 instrument with a LaB_6 filament furnished with a digital camera (Gatan) and operating at a voltage of 200 kV. The samples for TEM analysis were prepared by ultrasonicating an OMC powder suspension in acetone for 1 min. and capturing sample particles on a holey carbon-coated 300-mesh Cu grid by sweeping this through the suspension and then allowing the grid to dry under a halogen lamp overnight. Images were collected and analysed using Digital Micrograph software and Digital Diffraction Patterns (DDPs) were calculated by performing a Fourier Transform on selected areas of suitable images using the same software. SEM was carried out using a JEOL JSM-IT200 instrument and Energy Dispersive Spectroscopy (EDS) for chemical analysis was performed in this instrument using JEOL's integrated "live analysis" system. XPS spectra were obtained in survey scan mode and for C 1s, N 1s, O 1s and Na 1s regions using the Scienta spectrometer at the University of St Andrews and data were

processed using CASAS software. Fourier Transform Infrared (FT-IR) spectra were obtained on an IRAffinity-1S instrument (M/s Shimadzu, Japan) operated using LabSolutions IR software. Before each measurement, a background spectrum was recorded. Solid-state ^{13}C NMR spectra were recorded on a Bruker Avance III spectrometer equipped with a 9.4 T wide-bore superconducting magnet (^{1}H, Larmor frequency- 400.1 MHz and ^{13}C, Larmor frequency- 100.6 MHz).

2.3 Adsorption Experiments

MO, a water-soluble, mono-azo anionic dye, IUPAC name- Sodium 4-dimethylaminoazobenzene-4-sulphonate, molecular formula- $C_{14}H_{14}N_3NaO_3S$, molecular weight- 327.34 g/mol, was obtained from M/s Merck, India. HCl and NaOH used for the pH adjustments were also procured from M/s Merck, India. The reagents were used without any further purification. Double-distilled water, prepared in the laboratory, was used in all experiments. The pH of the solutions was determined using a digital pH meter (microprocessor-based) by M/s Hanna Instruments, Italy. A 0.01 M stock solution of the dye was prepared and the studies were carried out using the dilution solutions obtained from it. The absorbance of the dye solutions, in both batch and column operations, was recorded using a UV-Vis Spectrophotometer purchased from M/s EI, India.

2.3.1. Batch Experiments

The batch experiments were carried out by selecting a dye concentration range of 1×10^{-5} M to 6×10^{-5} M. 20 cm^3 volumes of dye solution, with a fixed dose of adsorbent, were placed in 100 mL Erlenmeyer flasks and were agitated using a water bath shaker. The influence of pH on the adsorption process was studies over the pH range 2-11. The initial and equilibrium concentrations of dye were determined by measuring the absorbance of the solutions before and after dye adsorption at the maximum absorption wavelength of MO (463 nm). The adsorption capacity at equilibrium was calculated using equation (1):

$$q_e = \frac{(C_0 - C_e) \times V}{w} \qquad (1)$$

where C_0 represents the pre-adsorption concentration and C_e refers to the equilibrium concentration of the dye in mol.L^{-1}, V is the volume of the solution mixture in litres and w represents the mass in g of the adsorbent employed.

The same procedure was applied for the kinetic and isothermal experiments. A specific amount of OMC as determined in the preliminary investigations was added to 20 mL dye solution of predetermined concentration and shaken on a water bath in an isothermal environment i.e., at 303 K, 313 K, and 323 K.

2.3.2. Column Experiments

A fixed-bed column of the material was prepared, supported on glass wool, in a glass column of 30 cm height and 1 cm internal diameter. To make the column, a slurry was made by dispersing 0.2 g of the OMC material in 1 litre of double-distilled water and the slurry was then left overnight. To avoid any air-entrapment, a jet of double-distilled water was made to travel through the column before adding the slurry to it. The slurry eas then introduced into the glass column in a careful manner which led to the settling of the particles and the formation of a fixed-bed of the mesoporous material, replacing the water that had been passed through the column previously.

Once a steady feed of the solution into the column had been established, 10 mL samples of the solution were collected and their respective dye concentrations were found using a UV-Visible spectrophotometer. A higher concentration was recorded for each successive sample and the operation was continued until the sample dye concentration was equal to the initial concentration.

After the complete exhaustion of the column, column-reusability tests were carried out. To desorb the adsorbed dye, 2-Methoxy ethanol was passed through the column at a flow rate of 0.5 mL/min. The selection of this eluent was based on the fact that the solubility of

MO in it is four times its solubility in water at 20 °C (solubility in water- 0.5 g/100 mL; in 2-Methoxy ethanol- 2 g/100 mL). The operation were performed until no dye was detected in the collected sample, when it was assumed that removal of the dye was complete. The same procedure was adopted for consecutive adsorption-desorption cycles.

3. Results and Discussions

This section describes the characterisation of the OMC materials and presents the evaluation of their potential for removing MO from water together with detailed interpretation of these results.

3.1 Material Characterization

The Type IV isotherm obtained in the nitrogen physisorption experiments exhibited H1 hysteresis and sharp capillary condensation in the relative pressure range of 0.4-0.8. This confirmed that the material consisted of cylindrical mesopores (Figure 2a). The physisorption data were used to determine the specific surface area (608 m^2g^{-1}) and the specific pore volume (0.63 cm^3g^{-1}) of the material. The data were also used to obtain a pore size distribution plot for the OMC material. A single, distinct, narrow peak was observed which implies a narrow pore size distribution, and this was centred at a value of 7.0 nm (Figure 2b).

The bulk material of the OMC product was prepared by polymerization followed by calcination at the relatively low temperature of 400°C and can therefore be considered to be essentially disordered, amorphous, or non-crystalline (Lu et al., 2008). However, the material does give rise to X-ray diffraction peaks at small angles. These are related to scattering from the periodically-ordered planes of pores in the ordered mesopore structure of the material. The SAXRD pattern of the OMC is given in Figure 2c. The peaks observed can be indexed to the 100, 200, 210 Miller planes of the parallel, cylindrical pores expected to comprise a two-dimensional hexagonal pore structure in the OMC. The positions of the indexed peaks in the

SAXRD pattern were used to calculate the unit cell dimension of the ordered mesopore structure using Bragg's Law, and this was found to be 13 nm (Figure 2c).

The TEM images obtained at a range of magnifications can be seen in Figure 2d-i. The carbon-containing matrix appears dark and the mesopores appear white. In Figure 2d-f it is clear that the material consists of long, parallel pores of uniform diameter and that these show long-range order. These images all show the pores in 'side-on' view at increasing magnifications. Figure 2g-i, show the highly ordered hexagonal arrangement of the cylindrical mesopores when these are viewed 'end-on. The hexagonal arrangement of pores is clear in the images and can be further confirmed by calculating DDPs from selected areas of the images, as is shown for images (g) and (h) The sharpness of the diffraction spots and the clarity of these diffraction patterns is further, strong evidence for the highly ordered, hexagonal arrangement of the mesopores.

SEM images are presented in Figure 3 for both the as-prepared OMC and OMC-MO, the OMC material after stirring for 3 h with aqueous MO solution, filtering and drying overnight at 60 °C. The images show angular OMC particles of size in the sub-micron to few micron range. In both images the surfaces of the particles exhibit uniform roughness which can be attributed to their mesoporous nature. Chemical analysis by EDS in the SEM instrument detected only C (77 wt%) and O (23 wt%) in the OMC but C (71 wt%), slightly more O (29 wt%) and some S (0.1 wt%), attributed to the presence of MO, in the OMC-MO. There is no obvious effect on the SEM images of the presence of the OMC, however.

To study the chemical nature of the OMC material, FT-IR and NMR spectra were recorded. Figure 4a presents the FT-IR spectrum of the as-prepared OMC adsorbent material. The bands in the range 1300 - 1000 cm^{-1} can be assigned to the in-plane bending of the C-H bonds in the aromatic rings while bands at 1609 and 1445 cm^{-1} correspond to C-C stretching in the aromatic rings. The band at around 1100 cm^{-1} is assigned to the C-O stretch in the

phenolic resin, and the presence of the OH group is indicated by a broad, weak band at about 3468 cm^{-1}. In Figure 4b the FTIR spectra of OMC, pure MO and OMC-MO are compared over the wavenumber range, 500-2100 cm^{-1}. Several of the major MO peaks in this range are seen in the spectrum of OMC-MO - specifically at around 1515, 1360, 1310, 1035, 1005, 945, 810 and 690 cm^{-1} (as indicated in the figure) – confirming the presence of MO, but their intensities are very low, precluding more detailed analysis. Interestingly, in XPS, when the N 1s peak was used to check for the presence of MO on the surface of OMC-MO, the intensity was found to be very low or zero (i.e. within the noise levels, data not presented). XPS is an extreme surface technique (sensitive only to the top few nm of a sample surface) whereas EDS and FTIR, as used here, probe much deeper into the bulk of the sample. Therefore, the N 1s XPS results together with the fact that MO was detected in both FTIR and EDS suggest that the MO was largely absorbed into the mesopores of the OMC material, leaving only low concentrations on the external surface. This is consistent with the similarity of the SEM images for OMC and OMC-MO, and that no agglomerations or crystals of MO were evident in the latter.

Raman spectra could not be obtained in the current study because of excessive fluorescence. However, a recent detailed Raman study on OMCs made using the same precursors - but possessing an ordered body-centred cubic pore structure - showed roughly equal proportions of single C–C bonds (sp^3 hybridised carbon) and of aromatic C=C multiple bonds (sp^2 hybridised C, termed ‘graphitic’) in the sample prepared at 400°C (Sakina and Baker, 2021). The OMC of the current study would be expected to show a similar ratio.

The ^{13}C CP MAS NMR spectra of the as-prepared OMC material can be seen in Figure 4c. Spectral assignments follow the numbering scheme shown in the representative chemical structure included in the figure and are based on previous assignments of Meng et al. (Meng et al., 2006). The appearance of the peak at ~ 152 ppm confirms the presence of the

-OH group in the material and this helps in predicting the possible mechanism of adsorption of MO.

3.2 Batch Experiments

The preliminary adsorption tests, isotherm measurements, and kinetic investigations that comprised the batch experiments are presented in this section.

3.2.1 Preliminary Investigations

It is imperative to investigate the values of various process variables for optimum exploitation of the potential of any adsorbent. The influence of various parameters on the uptake of MO by OMC was studied and the results are discussed in the following sub-sections.

3.2.2.1 Influence of pH

The effect of pH on the adsorption of MO on the OMC was investigated over a pH range of 2-11. It can be seen in Figure 5 that an irregular trend was observed during the investigation. Initially, when the pH was increased from 2 to 4, a rise in the removal efficiency was observed. At pH 5.0, the curve saw a dip but the removal efficiency increased again with a rise in pH up to 7.0. An explanation for this is that at pH just above the optimum pH there may be excessive competition among the MO molecules/ions for adsorption sites. This would cause mutual repulsion and the adsorption of MO is disfavoured. As the pH reaches pHpzc, the competition may decrease due to the neutrality of the surface of the OMC thereby improving the adsorption of MO, which then continues in the neutral medium. A further increase in pH however was accompanied by a decrease in the removal efficiency. Moreover, the highest removal efficiency was observed at pH 4.0. Because of this, all the following batch, as well as column studies, were carried out at pH 4.0.

The point of zero charge of the OMC, pH_{PZC}, determined by the salt addition method (Cardenas Peña et al., 2012; A. A. Hamad et al., 2020), was found to be 6.0. It is well

established that the surface of the adsorbent bears a positive charge when the pH of the medium is less than the pH_{PZC} and has a net negative charge if the pH of the medium is above pH_{PZC} (Hamadi et al., 2021; Tang and Ahmad Zaini, 2020; Xiao et al., 2021). The pKa of MO has been determined to be 3.46 (Kolthoff, 2002). The highest value of the removal efficiency was obtained at a pH of 4.0 and could be due to the strong electrostatic interactions between the ionized MO species and the positively charged adsorbent surface. The acidic environment favoured the adsorption of another anionic dye onto tea leaf residue (Jain et al., 2020). The removal percentage in a neutral medium is only slightly less than that at pH 4.0. This indicates that the adsorbent is still effective in a neutral medium, without the need to adjust the pH of the medium. The decrease in the adsorption efficiency beyond pH 7.0 can be attributed to repulsion between the negatively-charged adsorbent surface and the anionic dye. The interaction between the protonated -OH groups present on the surface of the adsorbent (as determined from the ^{13}C NMR) at pH 4.0 and the sulphonate groups on the dye, along with the pi-pi stacking interactions, maybe controlling the adsorption.

3.2.2.2 Influence of Adsorbent Quantity

The amount of adsorbent influences the adsorption process to a great extent. To determine the amount of the OMC sufficient to obtain maximum adsorption capacity, the influence of the dosage of adsorbent was investigated by utilising varying amounts of adsorbent, viz. 5-20 mg. In Figure 6, it is shown how the removal efficiency increased continuously as the adsorbent dose was increased. When the adsorbent dosage is increased, the surface area and the number of active sites increase, thereby increasing the removal efficiency (El-Sayed et al., 2020).

A rapid rise in the removal efficiency was observed when the amount was increased from 5 mg (85 %) to 10 mg (94.5 %). Thereafter, the rise in removal efficiency was gradual and approached 98.8 % at an adsorbent dosage of 20 mg. There was no further increase in the

adsorption efficiency and the value remained constant beyond 20 mg. An amount of 20 mg of adsorbent was thereforefixed for the subsequent batch experiments.

3.2.2.3 Influence of Dye Concentration

The initial concentration of dye is another important factor that influences the process of adsorption by developing a concentration gradient, along which the diffusion of dyes from the bulk solution to the surface of the adsorbent occurs. The effect of the concentration of MO on its removal by the OMC was studied over a range of 1×10^{-5} M to 6×10^{-5} M. In Figure 7, it is seen that, initially, a rise in the initial concentration favoured the adsorption of the dye causing an increase in the removal efficiency (92.36 % at 1×10^{-5} M and 98.8 % at 5×10^{-5} M). However, above a concentration of 5×10^{-5} M, a fall in the removal efficiency was witnessed (96.6 % at 6×10^{-5} M). This may be due to overcrowding of the dye moieties at the solid-solution surface and thus, to increased competition preventing the efficient adsorption of the adsorbate. The uptake of Methyl Orange by an adsorbent fabricated from industrial carpet waste showed a similar behaviour (Janbooranapinij et al., 2021). The other preliminary studies were then carried out with a dye concentration of 5×10^{-5} M.

3.2.2.4 Influence of Phase Contact Time

Keeping the pH of the medium fixed at 4.0 and the dye concentration at 5×10^{-5} M, 20 mL of the dye solution was shaken with 20 mg of the adsorbent, and samples were withdrawn at regular intervals to record their absorbance. This allowed the determination of the time required for the establishment of equilibrium. The removal efficiency increased quite rapidly in the first 30 min., reaching 63.4% (Figure 8). This was followed by a gradual rise from 45 min. (66.2 %) up to 210 min. (98.8 %) from where the flattening of the curve began (Eltarahony et al., 2021). This marked the attainment of equilibrium. The steady rise in the removal efficiency to a plateau may be attributed to the progressive saturation of the active

sites over time, lowering the number of available vacant sites due to their occupancy by the already adsorbed species.

3.2.2 Adsorption Kinetics

Studies on the kinetics of adsorption were carried out to determine the order of the reaction and also to elucidate the mechanism of adsorption along with the rate-controlling step of the overall process. The kinetic data were obtained by withdrawing samples from the MO-OMC system every fifteen min. The data obtained were then interpreted by fitting them to the linear expressions of pseudo-first-order (PFO) and pseudo-second-order (PSO) kinetic models (Helfferich and Dranoff, 1963; Ho and McKay, 1999a). The equation of the PFO model is expressed as Equation 2 and that of the PSO model is shown as Equations 3. In the expressions, q_e is the equilibrium adsorption capacity, q_t is the adsorption capacity at time 't', and k_1 (min^{-1}) is the pseudo-first-order rate constant and k_2 ($g.mol^{-1}min^{-1}$) represents the pseudo-second-order rate constant.

$$\log(q_e - q_t) = \log q_e - \frac{k_1}{2.303} \times t \qquad (2)$$

$$\frac{t}{q_t} = \frac{1}{k_2 q_e^2} + \frac{t}{q_e} \qquad (3)$$

The suitability of the model was determined from the regression coefficient values which were higher for the PSO model (>0.99) (Figure 9). For this reason, the adsorption of MO on the OMC was assumed to follow pseudo-second-order kinetics. The adsorption of another anionic azo dye, acid orange 7, onto activated carbon derived from extracted coffee residues was also reported to follow pseudo-second-order kinetics (Jung et al., 2017). The calculated values of pseudo-second-order constants are listed in Table 1. The values of k_2 increased with temperature whereas the half-life decreased.

3.2.3 Mechanism of Adsorption

As stated earlier, the kinetic data were used to study the overall adsorption controlling step. Well-established mathematical approaches described by Boyd (Boyd et al., 1947) and

Reichenberg (Reichenberg, 1953) were adopted for the interpretation of the kinetic data. The process of adsorption of the adsorbate species of any sort occurs in a set of three sequential steps: a) *film diffusion* whereby adsorbate species diffuse from the bulk solution to the adsorbent surface; b) *particle diffusion* in which adsorbate species diffuse within the adsorbent pores; c) adsorption of adsorbate species on the internal surface of the adsorbent. The third step proceeds so fast that its chances of being rate-determining are negligible (Crank, 1956). Thus, either step 'a' or 'b' is expected to be rate-limiting with the following three possibilities: when the rate of external diffusion is greater than the rate of internal diffusion, film diffusion is considered to be rate-limiting; when the rate of internal transport is higher than that of external transport, particle diffusion is assumed to be the rate-controlling step. When the external and the internal transport rates are approximately equal, there forms a liquid film at the bulk solution-adsorbent interface resulting in the development of a concentration gradient sufficient to prevent further adsorption.

The quantitative treatment of the sorption kinetics was undertaken by applying proper boundary conditions and using the following expressions as given by Reichenberg (Reichenberg, 1953):

$$F = \frac{Q_t}{Q_\infty} \qquad (4)$$

$$F = 1 - \frac{6}{\pi^2} \sum_{\infty}^{1} \left(\frac{1}{n^2}\right) e^{\left(-n^2 B_t\right)} \qquad (5)$$

$$B_t = \frac{\pi^2 D_i}{(r_0^2)} = Time\ constant \qquad (6)$$

where, Q_t is adsorption capacity in $mol.g^{-1}$ after time t, whereas Q_∞ is the adsorption capacity after infinite time, F represents the degree of attainment of equilibrium (fractional) at time t, n is the Freundlich constant, B_t represents the time whose values are noted corresponding to each F value, from Reichenberg's table (Reichenberg, 1953), D_i is the effective diffusion

coefficient within the adsorbent pores ($cm^2.s^{-1}$) and r_o is the radius of the adsorbent particle (assumed to be spherical).

To examine the diffusion mechanism in the MO-OMC system, a graph of B_t against time was plotted (Figure 10). Straight lines at all temperatures, viz., 303 K, 313 K, and 323 K, which cut the origin were obtained, indicating the involvement of particle diffusion as the rate-determining step (Reichenberg, 1953). Additionally, the slope of the plot gives the effective diffusion constant, D_i, the values of which increased with increasing temperature. This increase with temperature is attributed to a decrease in the retarding force acting on the diffusing dye moieties and also to their increased mobilities. A graph relating ln D_i to the reciprocal of temperature, 1/T, was plotted (Figure 11) to allow calculation of the maximum diffusion coefficient, D_0 ($cm^2.s^{-1}$), the energy of activation E_a ($kJ.mol^{-1}$), and the entropy of activation ($\Delta S^{\#}$), using the following expressions (Equations 7 and 8), where R and T have their usual significance, d represents the distance between two successive surface sites on the adsorbent, k is the Boltzmann factor (1.38×10^{-23} $J.K^{-1}$), and h is Plank's constant (6.62×10^{-34} J.s).

$$D_i = D_0 e^{\left(-\frac{E_a}{RT}\right)} \quad (7)$$

$$D_0 = \left(\frac{2.72\, d^2 kT}{h}\right) e^{\frac{\Delta S^{\#}}{R}} \quad (8)$$

The value of the energy of activation was calculated to be 7.248 $kJ.mol^{-1}$ and the positive entropy of activation indicates a high affinity of MO towards the OMC. All the values are recorded in Table 2.

Validation of the results obtained by interpreting the B_t versus time plot was carried out by obtaining a Ho and MacKay plot of log (1-F) versus time (Figure 12). The resulting non-linear plots at the different temperatures used further confirmed that the adsorption of MO on the OMC proceeded through particle-diffusion (Ho and McKay, 1999b, 1999a).

The experimental data were then analysed by applying the intra-particle diffusion model proposed by Weber and Morris. The mathematical equation of the model is expressed as-

$$q_t = K_{id} t^{0.5} + C_{id} \qquad (9)$$

where K_{id} (mol.g^{-1}.min$^{-1/2}$) refers to the intra-particle diffusion constant and the value of the constant C_{id} is proportional to the thickness of the boundary layer formed at the liquid-solid interface. As seen in Figure 13, when q_t values were plotted against $t^{0.5}$, the curves obtained were linear ($R^2 > 0.98$) with no significant intercept value showing the predominance of particle diffusion. The results complied with those obtained from B_t versus time plots. (Ali et al., 2016; El Kady et al., 2016).

3.2.4 Adsorption Isotherms

The development of any efficient adsorption system depends on understanding its behaviour in the context of various adsorption isotherm models. It is imperative to attempt to fit the experimental data to a range of adsorption isotherm models to identify the model that best explains the data. In this study, the applicability of Langmuir, Freundlich, Temkin, and Dubinin-Radushkevitch models was tested (Adamson et al., 1967; Masel, 1996; Mathias et al., 1996).

The assumptions that form the basis of the Langmuir isotherm model are that the adsorbate species are adsorbed on a homogeneous surface of the adsorbent in such a way that a monolayer is formed. Also, it is assumed that the adsorbed moieties do not undergo any mutual interactions. The linearized expression for the Langmuir adsorption model is presented as Equation 9.

$$\frac{1}{q_e} = \frac{1}{q_0} + \frac{1}{b q_0 C_e} \qquad (9)$$

where b stands for Langmuir constant ($L.mol^{-1}$), q_e for equilibrium adsorption capacity ($mol.g^{-1}$), q_0 for maximum adsorption capacity ($mol.g^{-1}$), and C_e for the equilibrium concentration of dye solution ($mol.L^{-1}$).

Plots of $1/q_e$ versus $1/C_e$ (Figure 14) were obtained with high values of regression coefficient at all temperatures (>0.98) (Elkady et al., 2019). However, the values showed a decreasing trend with increasing temperature. This suggests that the adsorption was typically monolayer at 303 K but as the temperature increased to 313 K and then to 323 K, the adsorption could not be described as strictly monolayer. Also, the values of the maximum adsorption capacity decreased with increasing temperature thereby suggesting the nature of the adsorption to be exergonic. The adsorption capacity values were reported to change in a similar way while studying the removal of the dye Tartrazine onto *Moringa oleifera* seeds (Reck et al., 2018).

The other most commonly applied model, the Freundlich model, assumes the heterogeneity of the surface and non-ideal, multilayer adsorption of the adsorbate. The possibility of mutual interactions of the adsorbate species affecting the adsorption is not ruled out and as a result, the sites having stronger binding affinities are the first to be occupied. Equation 10 shows the linearized Freundlich adsorption isotherm expression based on which, Figure 15 was plotted.

$$\log q_e = \log K_F + \left(\frac{1}{n}\right) \log C_e \qquad (10)$$

where the Freundlich constant K_F denotes the strength while n denotes the intensity of adsorption.

The values of the regression coefficient were high at high temperatures suggesting that at higher temperatures the adsorption of MO on the OMC might be multilayer (Figure 15). The values of 'n' at all the temperatures were found to be greater than unity, implying

the favourability of the process (El Essawy et al., 2017). The value of K_F however decreased with rising temperature.

The data were further analysed by applying the Temkin isotherm model that is based on the hypothesis that there might be indirect interactions between the adsorbed species. The Temkin adsorption isotherm equation is expressed as Equation 11.

$$q_e = k_1 \ln k_2 + k_1 \ln C_e \qquad (11)$$

where k_1 and k_2 are Temkin constants and k_1 is equal to RT/b, which represents the heat of adsorption, whereas k_2 is the binding constant at equilibrium. However, the low values of the regression constant indicate the non-applicability of this model in the case of the present system (Figure 16).

Lastly, the applicability of the Dubinin-Radushkevitch isotherm model was investigated by plotting graphs of ln q_e against ϵ^2 at different temperatures (Figure 17) where linear relationships were observed at all the temperatures studied. This model is employed to calculate the mean sorption energy and to estimate the porosity of the adsorbent. The linear form of the D-R adsorption isotherm expression is shown as Equation 12.

$$\ln q_e = \ln q_m - \beta\epsilon^2 \qquad (12)$$

where q_m is the maximum adsorption capacity (mol.g^{-1}), β is the activity coefficient, also called the D-R constant, the value of which is determined from the slope of D-R adsorption isotherm and is used to calculate the mean sorption energy, E (=1/√-2β). The Polanyi potential, ϵ, is given by:

$$\epsilon = RT\left(1 + \frac{1}{C_e}\right) \qquad (13)$$

where all the terms have their conventional meanings.

The significance of this isotherm model lies in the fact that it helps in ascertaining the nature of adsorption. That is, whether the process involves physisorption or chemisorption. If the calculated value of E is lower than 8 kJ, the adsorption involves physisorption and a value

of E between 8 and 16 kJ is indicative of the involvement of chemisorption as an overall rate-governing step. In the present case, the same value of E, i.e., 10 kJ was obtained at all temperatures (303 K, 313 K, and 323 K) suggesting the adsorption of MO on the OMC is through chemisorption. The values of all the adsorption isotherm constants are shown in Table 3.

3.2.5 Thermodynamics of Adsorption

The thermodynamics of any process can be studied based on the calculation of the fundamental thermodynamic parameters, change in Gibb's free energy (ΔG°), in enthalpy (ΔH°), and in entropy (ΔS°). The following well-established equations are employed for the estimation of the aforementioned thermodynamic variables:

$$\Delta G^0 = -RT \ln b \qquad (14)$$

$$\Delta H^0 = -R \left(\frac{T_2 T_1}{(T_2 - T_1)}\right) \times \ln\left(\frac{b_2}{b_1}\right) \qquad (15)$$

$$\Delta S^0 = \frac{(\Delta H^0 - \Delta G^0)}{T} \qquad (16)$$

A dimensionless quantity, r, also referred to as separation factor, is also used to ascertain the favourability of the reaction, which is given by (Weber and Chakravorti, 1974):

$$r = \frac{1}{1 + bC_0} \qquad (17)$$

For a reaction to be favourable, the value of r must fall between 0 and 1 ($0 < r < 1$). The calculated values of r for all the temperatures, viz., 303 K, 313 K, and 323 K, were less than unity, showing the favourability of the adsorption of MO on the OMC.

The values of the above-mentioned thermodynamic quantities and that of r are listed in Table 4. The negative values of change in Gibb's free energy, at 303 K, 313 K, and 323 K, indicate that the adsorption of MO on the OMC is spontaneous. The calculated changes in enthalpy were also negative at all test temperatures confirming further the results obtained from the Langmuir isotherm model, where the maximum adsorption capacity was found to

decrease as temperature increased. The calculated values of entropy change were also negative at all temperatures, indicating that the adsorption of the adsorbate ions/species had lowered the disorder at the solid-solution interface. Similar thermodynamic results were obtained for the removal of the dye Remazol Brilliant Blue R using denim waste-based mesoporous activated carbon fibres (Silva et al., 2018).

To sum up, the involvement of electrostatic attractive forces between the sulphonate groups on MO and protonated hydroxyl groups on the surface of OMC may be playing a prominent role based on the applicability of the pseudo-second-order model where there might be a transfer of electrons between MO and OMC. Isothermal studies revealed that the adsorption of MO on the surface of OMC may not be precisely monolayer. This indicates that apart from the dominating electrostatic interactions, pi-pi interactions between MO and OMC are also operative. The interpretation of thermodynamic results on the other hand also helps to determine the mechanism of MO adsorption. The high value of enthalpy change at low temperature (303 K) is indicative of strong forces acting between MO and OMC. The values of Gibb's free energy change show that the spontaneity of reaction increases with temperature (Elessawy et al., 2020).

3.3 Column Operations

The batch experiments are certainly useful to study the adsorption behaviour of any adsorbate-adsorbent system. Their limited practical applicability, however, makes column operations preferable. Column operations result in the bulk removal of the dye and are faster and more practicable. Because the adsorbate is fed continuously to the column, the concentration of the dye solution in contact with the column remains constant, resulting in the establishing of a higher concentration gradient across the adsorbate-adsorbent interface. This, in turn, improves the scavenging efficiency of the adsorbent giving rise to higher adsorption capacities than those attained in batch experiments (Chern and Chien, 2002).

The procedure involved in column operations has been discussed in Section 2.3.2. An S-shaped curve, referred to as the breakthrough curve was obtained by plotting the volume of eluted samples as abscissa and their concentration as ordinate (Figure 18). This breakthrough curve was then analysed to determine the adsorption efficiency based on the percentage saturation of the column. As observed in Figure 18, no or negligible amounts of dye were detected in the eluted samples up to 30 mL, followed by a smooth and constant rise to 290 mL, the point at which the curve started to flatten out. This marked the saturation of the column. The sigmoidal shape of the curve indicates that the adsorption efficiency was at its maximum initially and decreased progressively to the point of saturation. The saturation of the column starts from the upmost section of the column and a zone of uniform saturation, known as the primary adsorption zone, is formed. This zone travels down the length of the column and, in the present case, the movement of the primary adsorption zone resulted in almost the same concentration of dye in the exiting sample as was in the feed sample after a volume of 290 mL of the MO solution had been collected. This situation is called the point of exhaustion. The expressions that were employed for the interpretation of the breakthrough curve and the calculation of various parameters are as follows (Chern and Chien, 2002; Michaels, 1952):

$$t_x = \frac{V_x}{F_m} \tag{18}$$

$$t_\delta = \frac{V_x - V_b}{F_m} \tag{19}$$

$$\frac{\delta}{D} = \frac{t_\delta}{t_x - t_f} = \frac{t_\delta}{t_x + t_\delta(f-1)} = \frac{(V_x - V_b)}{V_b + f(V_x - V_b)} \tag{20}$$

$$f = 1 - \frac{t_f}{t_\delta} = \frac{M_s}{(V_x - V_b)C_0} \tag{21}$$

$$Percentage\ saturation = \frac{D + \delta(f-1)}{D} \times 100 \tag{22}$$

where, δ denotes the primary adsorption zone length, t_x = time in min. taken by the primary adsorption to form, t_δ = time (min.) taken by primary adsorption zone to travel down its length, t_f is the time in min. taken initially for the formation of the primary adsorption zone, C_x is the concentration at the point of column exhaustion and the corresponding volume is V_x (mL), V_b is the breakpoint volume, F_m is the mass flow rate, D the height of the fixed-bed, and f the fractional capacity of the column at the breakthrough point.

Various column parameters were calculated and their values are listed in Tables 5 and 6. Out of 98.199 mg of MO that was loaded into a column containing 0.2 g of adsorbent, 51.647 mg of the dye was adsorbed and 46.552 mg of the dye was collected unadsorbed. The primary adsorption zone took 39570.16 min. (t_x) to establish and the time it took (t_δ) to move down the column length (δ) was calculated to be 36932.15 min. The initial formation of the primary adsorption zone took 1319.00 min. The percentage saturation value as calculated from Equation 22 was found to be 96.55 %.

3.4 Column Regeneration

The ability of the column to regenerate was tested by desorbing the dye-loaded column using 2-Methoxy ethanol. The eluent was then made to travel through the column and the concentration of every 20 mL eluted sample was measured spectrophotometrically. The operation was continued until three concordant dye concentrations of the eluate exiting the column were obtained. It can be seen in Figure 19 that the desorption was stopped after the concentration of eluate remained unchanged from 440 mL to 480 mL. The percentage desorption was calculated and found to be equal to 93.26 %, indicating a strong interaction between MO and the OMC preventing its complete (100%) desorption. The adsorption capacity of the adsorbent, as discussed earlier, improved many-fold in column operations as compared to those obtained in batch studies and was found to be 258.2 $mg.g^{-1}$.

3.5 Column Efficacy

Three adsorption/desorption cycles were performed to test the efficacy of the column. For each cycle, the same procedure was repeated. Firstly, the dye solution of 1×10^{-3} M concentration, maintained at pH 4.0, was loaded into the column, followed by the latter's regeneration by 2-Methoxy ethanol. The efficiency of the column was evaluated in terms of percentage desorption. Figure 20 shows how the percentage desorption did not change dramatically and decreased only slightly from 93.26 % in the first cycle to 92.10 % in the third cycle.

4. Conclusion

The OMC material synthesised was found to consist of essentially amorphous, polymeric carbonaceous material but with a highly ordered arrangement of long, parallel, cylindrical mesopores of around 7 nm diameter. Spectrochemical analysis of the material using infrared and MAS-NMR methods showed that it contained aromatic and aliphatic carbon environments and C-H, C-OH, and $-CH_2-$ functional groups. These are expected to be present at the mesopore walls and are therefore important when considering the adsorption of dye molecules. The adsorption behaviour of MO on an OMC, developed via a metal and halogen-free route, was investigated. Through the preliminary experiments performed in batch mode, the values of various parameters were optimised (pH- 4.0, adsorbent dose- 20 mg/20 mL, dye concentration- 5×10^{-5} M, and contact time- 240 min). The Langmuir adsorption isotherm model was found to best fit the experimental data at 303 K. However, the Freundlich and the D-R adsorption isotherm models also showed fairly good fitting to the data. The adsorption of MO on the OMC was found to follow pseudo-second-order kinetics and the adsorption progressed predominantly through particle diffusion. The adsorption of MO on the OMC was thermodynamically favoured, spontaneous, and exergonic. The potential of the adsorbent was also tested in column operations and a column saturation of 96.55 % was achieved. The column was regenerated using a suitable eluent with a percentage

desorption equal to 93.26 %. Only a marginal decrease in column efficiency was observed after three cycles of adsorption-desorption. By all counts and with proven results, it is safe to assume that the present research provides an overview of the prospects of OMC in large-scale applications.

Acknowledgements

The authors are grateful to the Ministry of Human Resource Development of the Government of India for financial support through the SPARC Project- SPARC/2018-2019/P307/SL. One of the authors (Asna Mariyam) is also grateful to MANIT, Bhopal for providing fellowship assistance. We thank the University of St Andrews for a PhD scholarship for FS. Electron Microscopy was carried out at the Electron Microscopy Facility, School of Chemistry, University of St Andrews. We acknowledge EPSRC Strategic Resources Grant (EP/R023751/1).

References:

Adamson, A.W., Gast, A.P., others, 1967. Physical chemistry of surfaces. Interscience publishers New York.

Akansha, K., Chakraborty, D., Sachan, S.G., 2019. Decolorization and degradation of methyl orange by Bacillus stratosphericus SCA1007. Biocatalysis and Agricultural Biotechnology 18, 101044. https://doi.org/10.1016/J.BCAB.2019.101044

Ali, R.M., Hamad, H.A., Hussein, M.M., Malash, G.F., 2016. Potential of using green adsorbent of heavy metal removal from aqueous solutions: Adsorption kinetics, isotherm, thermodynamic, mechanism and economic analysis. Ecological Engineering 91, 317–332. https://doi.org/10.1016/j.ecoleng.2016.03.015

Anastopoulos, I., Mittal, A., Usman, M., Mittal, J., Yu, G., Núñez-Delgado, A., Kornaros, M., 2018. A review on halloysite-based adsorbents to remove pollutants in water and wastewater. Journal of Molecular Liquids 269, 855–868. https://doi.org/10.1016/J.MOLLIQ.2018.08.104

Beaudoin, A.R., Pickering, M.J., 1960. Teratogenic activity of several synthetic compounds structurally related to trypan blue. The Anatomical Record 137, 297–305.

Bharti, V., Vikrant, K., Goswami, M., Tiwari, H., Sonwani, R.K., Lee, J., Tsang, D.C.W., Kim, K.H., Saeed, M., Kumar, S., Rai, B.N., Giri, B.S., Singh, R.S., 2019. Biodegradation of methylene blue dye in a batch and continuous mode using biochar as packing media. Environmental Research 171, 356–364. https://doi.org/10.1016/J.ENVRES.2019.01.051

Bhattacharya, G., Sas, S., Wadhwa, S., Mathur, A., McLaughlin, J., Roy, S.S., 2017. Aloe vera assisted facile green synthesis of reduced graphene oxide for electrochemical and dye removal applications. RSC advances 7, 26680–26688. https://doi.org/10.1039/C7RA02828H

Boyd, G.E., Adamson, A.W., Myers Jr, L.S., 1947. The exchange adsorption of ions from aqueous solutions by organic zeolites. II. Kinetics1. Journal of the American Chemical Society 69, 2836–2848. https://doi.org/10.1021/ja01203a066

Cardenas Peña, A.M., Ibañez Cornejo, J.G., Vásquez Medrano, R.C., 2012. Determination of the point of zero charge for electrocoagulation precipitates from an iron anode. International Journal of Electrochemical Science 7, 6142–6153

Chang, J., Chadwick, R.W., Allison, J.C., Hayes, Y.O., Talley, D.L., Autry, C.E., 1994. Microbial succession and intestinal enzyme activities in the developing rat. Journal of Applied Bacteriology 77, 709–718. https://doi.org/10.1111/j.1365-2672.1994.tb02823.x

Chen, S., Zhang, J., Zhang, C., Yue, Q., Li, Y., Li, C., 2010. Equilibrium and kinetic studies of methyl orange and methyl violet adsorption on activated carbon derived from Phragmites australis. Desalination 252, 149–156. https://doi.org/10.1016/j.desal.2009.10.010

Chern, J.M., Chien, Y.W., 2002. Adsorption of nitrophenol onto activated carbon: isotherms and breakthrough curves. Water Research 36, 647–655. https://doi.org/10.1016/S0043-1354(01)00258-5

Chung, K.-T., 2000. Mutagenicity and carcinogenicity of aromatic amines metabolically produced from azo dyes. Journal of Environmental Science & Health Part C 18, 51–74. https://doi.org/10.1080/10590500009373515

Chung, K.T., 1983. The significance of azo-reduction in the mutagenesis and carcinogenesis of azo dyes. Mutation Research/Reviews in Genetic Toxicology 114, 269–281. https://doi.org/10.1016/0165-1110(83)90035-0

Chung, K.-T., Stevens, S.E., Cerniglia, C.E., 1992. The reduction of azo dyes by the intestinal microflora. Critical reviews in Microbiology 18, 175–190. https://doi.org/10.3109/10408419209114557

Crank, J., 1956. The mathematics of diffusion, 347 pp.

El Essawy, N.A., Ali, S.M., Farag, H.A., Konsowa, A.H., Elnouby, M., Hamad, H.A., 2017. Green synthesis of graphene from recycled PET bottle wastes for use in the adsorption of dyes in aqueous solution. Ecotoxicology and environmental safety 145, 57–68. https://doi.org/10.1016/j.ecoenv.2017.07.014

El Kady, M., Shokry, H., Hamad, H., 2016. Effect of superparamagnetic nanoparticles on the physicochemical properties of nano hydroxyapatite for groundwater treatment: Adsorption mechanism of Fe(II) and Mn(II). RSC Advances 6, 82244–82259. https://doi.org/10.1039/c6ra14497g

Elessawy, N.A., Elnouby, M., Gouda, M.H., Hamad, H.A., Taha, N.A., Gouda, M., Mohy Eldin, M.S., 2020. Ciprofloxacin removal using magnetic fullerene nanocomposite obtained from sustainable PET bottle wastes: Adsorption process optimization, kinetics, isotherm, regeneration and recycling studies. Chemosphere 239, 124728. https://doi.org/10.1016/j.chemosphere.2019.124728

Elkady, M., Shokry, H., El-Sharkawy, A., El-Subruiti, G., Hamad, H., 2019. New insights into the activity of green supported nanoscale zero-valent iron composites for enhanced acid blue-25 dye synergistic decolorization from aqueous medium. Journal of Molecular Liquids 294, 111628. https://doi.org/10.1016/j.molliq.2019.111628

El-Sayed, E.M., Hamad, H.A., Ali, R.M., 2020. Journey from ceramic waste to highly efficient toxic dye adsorption from aqueous solutions via one-pot synthesis of CaSO4 rod-shape with silica. Journal of Materials Research and Technology 9, 16051–16063. https://doi.org/10.1016/j.jmrt.2020.11.037

Eltarahony, M., Abu-Serie, M., Hamad, H., Zaki, S., Abd-El-Haleem, D., 2021. Unveiling the role of novel biogenic functionalized CuFe hybrid nanocomposites in boosting anticancer, antimicrobial and biosorption activities. Scientific Reports 11, 1–22. https://doi.org/10.1038/s41598-021-87363-z

Gang, D., Uddin Ahmad, Z., Lian, Q., Yao, L., Zappi, M.E., 2021. A review of adsorptive remediation of environmental pollutants from aqueous phase by ordered mesoporous carbon. Chemical Engineering Journal 403, 126286. https://doi.org/10.1016/J.CEJ.2020.126286

Golka, K., Kopps, S., Myslak, Z.W., 2004. Carcinogenicity of azo colorants: influence of solubility and bioavailability. Toxicology Letters 151, 203–210. https://doi.org/10.1016/J.TOXLET.2003.11.016

Gupta, V.K., Suhas, 2009. Application of low-cost adsorbents for dye removal – A review. Journal of Environmental Management 90, 2313–2342. https://doi.org/10.1016/J.JENVMAN.2008.11.017

Hamad, A.A., Hassouna, M.S., Shalaby, T.I., Elkady, M.F., Abd Elkawi, M.A., Hamad, H.A., 2020. Electrospun cellulose acetate nanofiber incorporated with hydroxyapatite for removal of heavy metals. International Journal of Biological Macromolecules 151, 1299–1313. https://doi.org/10.1016/J.IJBIOMAC.2019.10.176

Hamad, H., Bailón-García, E., Morales-Torres, S., Carrasco-Marín, F., Pérez-Cadenas, A.F., Maldonado-Hódar, F.J., 2020. Functionalized cellulose for the controlled synthesis of novel carbon-ti nanocomposites: Physicochemical and photocatalytic properties. Nanomaterials 10, 1–18. https://doi.org/10.3390/nano10040729

Hamadi, A., Yeddou-Mezenner, N., Lounis, A., Ali, R.M., Hamad, H., 2021. Upgrading of agro-industrial green biomass residues from chocolate industry for adsorption process: diffusion and mechanistic insights. Journal of Food Science and Technology 58, 1081–1092. https://doi.org/10.1007/s13197-020-04622-z

Hassan, M.M., Carr, C.M., 2018. A critical review on recent advancements of the removal of reactive dyes from dyehouse effluent by ion-exchange adsorbents. Chemosphere 209, 201–219. https://doi.org/10.1016/J.CHEMOSPHERE.2018.06.043

Helfferich, F.G., Dranoff, J.S., 1963. Ion Exchange, McGraw-Hill, New York (1962), 624 pp. $16.00.

Ho, Y.S., McKay, G., 1999a. Pseudo-second order model for sorption processes. Process Biochemistry 34, 451–465. https://doi.org/10.1016/S0032-9592(98)00112-5

Ho, Y.S., McKay, G., 1999b. The sorption of lead(II) ions on peat. Water Research 33, 578–584. https://doi.org/10.1016/S0043-1354(98)00207-3

Jadhav, S.A., Garud, H.B., Patil, A.H., Patil, G.D., Patil, C.R., Dongale, T.D., Patil, P.S., 2019. Recent advancements in silica nanoparticles based technologies for removal of dyes from water. Colloid and Interface Science Communications 30, 100181. https://doi.org/10.1016/J.COLCOM.2019.100181

Jain, S.N., Tamboli, S.R., Sutar, D.S., Jadhav, S.R., Marathe, J. v, Shaikh, A.A., Prajapati, A.A., 2020. Batch and continuous studies for adsorption of anionic dye onto waste tea residue : Kinetic

, equilibrium , breakthrough and reusability studies. Journal of Cleaner Production 252, 119778. https://doi.org/10.1016/j.jclepro.2019.119778

Janbooranapinij, K., Yimponpipatpol, A., Ngamthanacom, N., Panomsuwan, G., 2021. Conversion of industrial carpet waste into adsorbent materials for organic dye removal from water. Cleaner Engineering and Technology 4, 100150. https://doi.org/10.1016/j.clet.2021.100150

Joshni, T.C., Subramaniam, K., 2011. Enzymatic degradation of azo dyes-a review. International Journal of Environmental Sciences 1, 1250–1260.

Jung, K.W., Choi, B.H., Hwang, M.J., Choi, J.W., Lee, S.H., Chang, J.S., Ahn, K.H., 2017. Adsorptive removal of anionic azo dye from aqueous solution using activated carbon derived from extracted coffee residues. Journal of Cleaner Production 166, 360–368. https://doi.org/10.1016/j.jclepro.2017.08.045

Kanwal, A., Bhatti, H.N., Iqbal, M., Noreen, S., 2017. Basic dye adsorption onto clay/MnFe2O4 composite: a mechanistic study. Water Environment Research 89, 301–311. https://doi.org/10.2175/106143017X14839994522984

Kolthoff, I.M., 2002. Indicator constants. The Journal of Physical Chemistry 34, 1466–1483. https://doi.org/10.1021/j150313a008

Liu, L., Zhang, J., Tan, Y., Jiang, Y., Hu, M., Li, S., Zhai, Q., 2014. Rapid decolorization of anthraquinone and triphenylmethane dye using chloroperoxidase: Catalytic mechanism, analysis of products and degradation route. Chemical Engineering Journal 244, 9–18. https://doi.org/10.1016/J.CEJ.2014.01.063

Lu, A.-H., Spliethoff, B., Schüth, F., 2008. Aqueous synthesis of ordered mesoporous carbon via self-assembly catalyzed by amino acid. Chemistry of Materials 20, 5314–5319. https://doi.org/10.1021/cm800362g

Masel, R.I., 1996. Principles of adsorption and reaction on solid surfaces. John Wiley & Sons.

Mathias, P.M., Kumar, R., Moyer, J.D., Schork, J.M., Srinivasan, S.R., Auvil, S.R., Talu, O., 1996. Correlation of multicomponent gas adsorption by the dual-site Langmuir model. Application to nitrogen/oxygen adsorption on 5A-zeolite. Industrial \& engineering chemistry research 35, 2477–2483. https://doi.org/10.1021/ie950291y

Meng, Y., Gu, D., Zhang, F., Shi, Y., Cheng, L., Feng, D., Wu, Z., Chen, Z., Wan, Y., Stein, A., others, 2006. A family of highly ordered mesoporous polymer resin and carbon structures from organic- organic self-assembly. Chemistry of materials 18, 4447–4464. https://doi.org/10.1021/cm060921u

Michaels, A.S., 1952. Simplified method of interpreting kinetic data in fixed-bed ion exchange. Industrial & Engineering Chemistry 44, 1922–1930. https://doi.org/10.1021/ie50512a049

Mohan, D., Pittman Jr, C.U., Steele, P.H., 2006. Pyrolysis of wood/biomass for bio-oil: a critical review. Energy & Fuels 20, 848–889. https://doi.org/10.1021/ef0502397

Nidheesh, P. v., Zhou, M., Oturan, M.A., 2018. An overview on the removal of synthetic dyes from water by electrochemical advanced oxidation processes. Chemosphere 197, 210–227. https://doi.org/10.1016/J.CHEMOSPHERE.2017.12.195

Omar, H.H., 2008. Algal decolorization and degradation of monoazo and diazo dyes. Pakistan Journal of Biological Sciences 11, 1310–1316.

Rajabi, M., Mahanpoor, K., Moradi, O., 2017. Removal of dye molecules from aqueous solution by carbon nanotubes and carbon nanotube functional groups: critical review. RSC Advances 7, 47083–47090. https://doi.org/10.1039/C7RA09377B

Reck, I.M., Paixão, R.M., Bergamasco, R., Vieira, M.F., Vieira, A.M.S., 2018. Removal of tartrazine from aqueous solutions using adsorbents based on activated carbon and Moringa oleifera seeds. Journal of Cleaner Production 171, 85–97. https://doi.org/10.1016/j.jclepro.2017.09.237

Reichenberg, D., 1953. Properties of ion-exchange resins in relation to their structure. III. Kinetics of exchange. Journal of the American Chemical Society 75, 589–597. https://doi.org/10.1021/ja01099a022

Sadik, W.A., El-Demerdash, A.G.M., Nashed, A.W., Mostafa, A.A., Hamad, H.A., 2019. Highly efficient photocatalytic performance of Cu2O@TiO2 nanocomposite: influence of various inorganic oxidants and inorganic anions. Journal of Materials Research and Technology 8, 5405–5414. https://doi.org/10.1016/J.JMRT.2019.09.007

Sakina, F., Baker, R.T., 2021. Ordered mesoporous carbons with body centred cubic pore structure. Carbon Trends 4, 100051. https://doi.org/10.1016/J.CARTRE.2021.100051

Sakina, F., Baker, R.T., 2019. Metal- and halogen-free synthesis of ordered mesoporous carbon materials. Microporous and Mesoporous Materials 289, 109622. https://doi.org/10.1016/J.MICROMESO.2019.109622

Silva, T.L., Cazetta, A.L., Souza, P.S.C., Zhang, T., Asefa, T., Almeida, V.C., 2018. Mesoporous activated carbon fibers synthesized from denim fabric waste: Efficient adsorbents for removal of textile dye from aqueous solutions. Journal of Cleaner Production 171, 482–490. https://doi.org/10.1016/j.jclepro.2017.10.034

Soares, O.S.G.P., Órfão, J.J.M., Portela, D., Vieira, A., Pereira, M.F.R., 2006. Ozonation of textile effluents and dye solutions under continuous operation: Influence of operating parameters. Journal of Hazardous Materials 137, 1664–1673. https://doi.org/10.1016/J.JHAZMAT.2006.05.006

Tang, S.H., Ahmad Zaini, M.A., 2020. Development of activated carbon pellets using a facile low-cost binder for effective malachite green dye removal. Journal of Cleaner Production 253, 119970. https://doi.org/10.1016/j.jclepro.2020.119970

Tsuboy, M.S., Angeli, J.P.F., Mantovani, M.S., Knasmüller, S., Umbuzeiro, G.A., Ribeiro, L.R., 2007. Genotoxic, mutagenic and cytotoxic effects of the commercial dye CI Disperse Blue 291 in the human hepatic cell line HepG2. Toxicology in Vitro 21, 1650–1655. https://doi.org/10.1016/J.TIV.2007.06.020

Weber, T.W., Chakravorti, R.K., 1974. Pore and solid diffusion models for fixed-bed adsorbers. AIChE Journal 20, 228–238. https://doi.org/10.1002/aic.690200204

Wong, P.W., Teng, T.T., Norulaini, N.A.R.N., 2007. Efficiency of the coagulation-flocculation method for the treatment of dye mixtures containing disperse and reactive dye. Water Quality Research Journal 42, 54–62. https://doi.org/10.2166/wqrj.2007.008

Wu, Z., Zhao, D., 2011. Ordered mesoporous materials as adsorbents. Chemical Communications 47, 3332–3338. https://doi.org/10.1039/C0CC04909C

Xiao, W., Jiang, X., Liu, X., Zhou, W., Garba, Z.N., Lawan, I., Wang, L., Yuan, Z., 2021. Adsorption of organic dyes from wastewater by metal-doped porous carbon materials. Journal of Cleaner Production 284, 124773. https://doi.org/10.1016/j.jclepro.2020.124773

TABLES

Table 1. Values of Various Pseudo-Second-Order Kinetic Constants for the Adsorption of MO onto the OMC at Different Temperatures

Pseudo-second-order constants					
k_1 (g.mol^{-1}.min^{-1}) × 10^2			$t_{1/2}$ (min.)		
30°C	40°C	50°C	30°C	40°C	50°C
7.63	8.11	8.41	26.20	24.65	23.77

Table 2. Values of Diffusion Coefficients (D_i And D_0), Energy of Activation (E_a), Entropy ($\Delta S^{\#}$)

D_i (m^2/min)			D_0 (m^2/min)	E_a (J mol^{-1})	$\Delta S^{\#}$ (JK^{-1} mol^{-1})
30 °C	**40 °C**	**50 °C**			
1.63×10^{-2}	1.70×10^{-2}	1.95×10^{-2}	0.28	7248.89	11.00

Table 3. Values of Various Adsorption Isotherm Constants for the Uptake of MO by OMC at Different Temperatures

Langmuir Constants					
$q_0 \times 10^{-3}$ (mmol/g)			**$b \times 10^4$ ($L.mol^{-1}$)**		
30°C	40°C	50°C	30°C	40°C	50°C
0.33	0.096	0.075	1.22	5.83	9.01
Freundlich Constants					
n			**K_F**		
30°C	40°C	50°C	30°C	40°C	50°C
1.105	1.172	1.253	1.20	0.716	0.391
Temkin Constants					
$k_1 \times 10^{-5}$			**k_2 ($\times 10^5$)**		
30°C	40°C	50°C	30°C	40°C	50°C
2.00	2.00	2.00	5.00	5.00	5.00
D-R Constants					
X_m (mmol/g)			**β ($\times 10^{-9}$)**		
30°C	40°C	50°C	30°C	40°C	50°C
4.82	3.56	3.13	5.00	5.00	5.00

Table 4. Values of Various Thermodynamic Parameters for the Adsorption of MO by OMC at Different Temperatures

Temperature (^oC)	$-\Delta G°$ ($kJ.mol^{-1}$)	$-\Delta H°$ ($kJ.mol^{-1}$)	$-\Delta S°$ ($JK^{-1}mol^{-1}$)	r values
30	23.71	123.15	328.20	0.621
40	27.64	36.61	28.64	0.255
50	30.64	81.26	156.74	0.186

Table 5. Input Data for Calculations of MO - OMC Fixed Bed Adsorber Parameters

C_o (M)	C_x (M)	C_b (M)	V_x (mL)	V_b (mL)	$(V_x - V_b)$ (mL)	F_m (mg/cm^2)	D (cm)
1×10^{-3}	9.96×10^{-4}	3.7×10^{-6}	290	10	280	0.00758	0.5

Table 6. Values of Parameters of MO - OMC Fixed Bed Adsorber

t_x (min)	t_δ (min)	t_f (min)	f	δ (cm)	Percentage Saturation
39570.16	36932.15	1319.00	0.964	0.482	96.55

FIGURES

Figure 1. **Schematic representation of the preparation of the OMC material used as the adsorbent in this study**

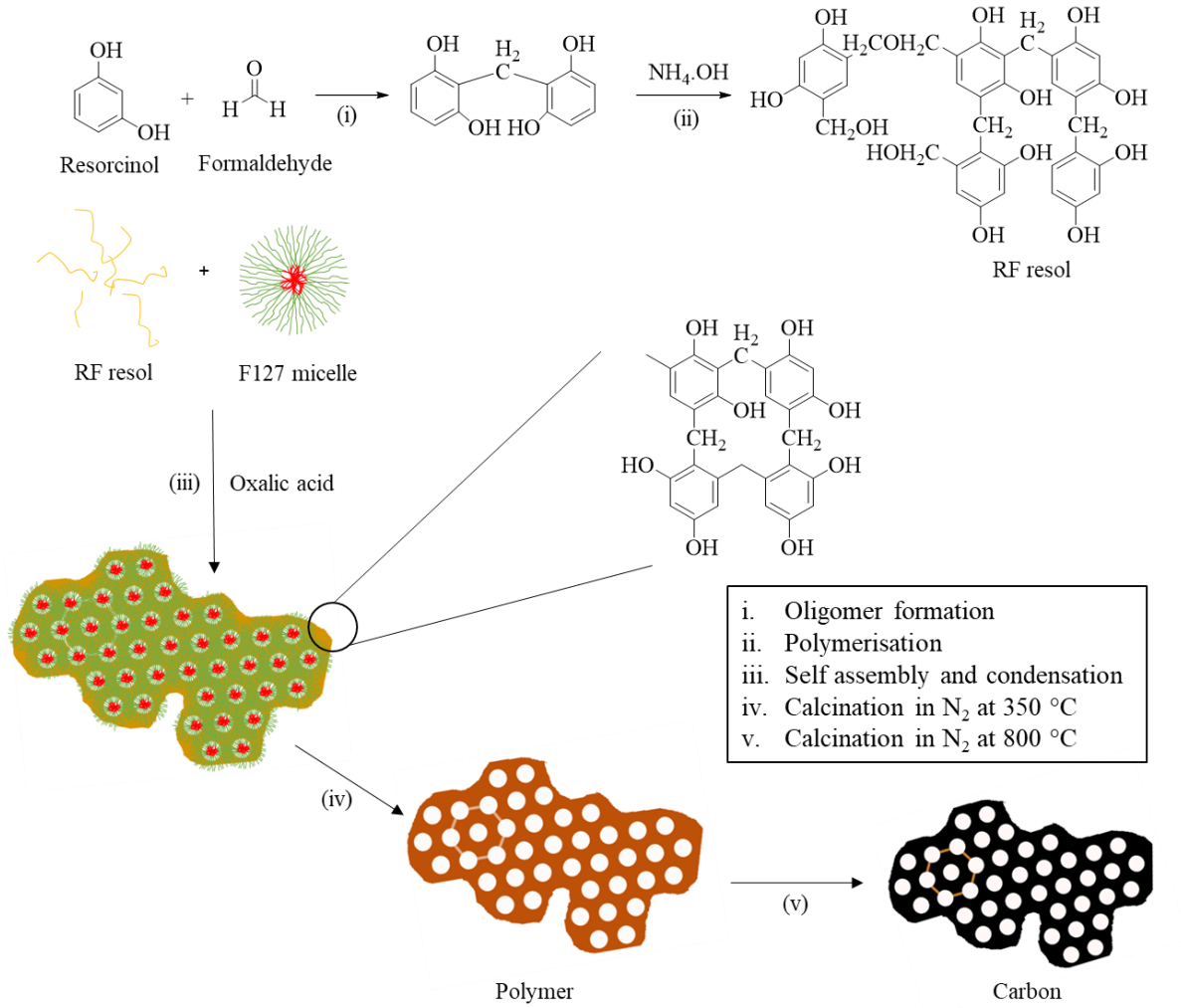

Figure 2. **Physical characterisation of the OMC material: gas physisorption isotherm (a); distribution of pore size calculated from the isotherm; SAXRD pattern with the major planes of the pore structure indexed (c). TEM images at increasing magnification showing: extensive ordering of parallel cylindrical pores in side-on view (d,e,f); and in end-on view, showing the hexagonal arrangement of mesopores. DDPs of the ordered pore structure are inset and indexed for images (g) and (h).**

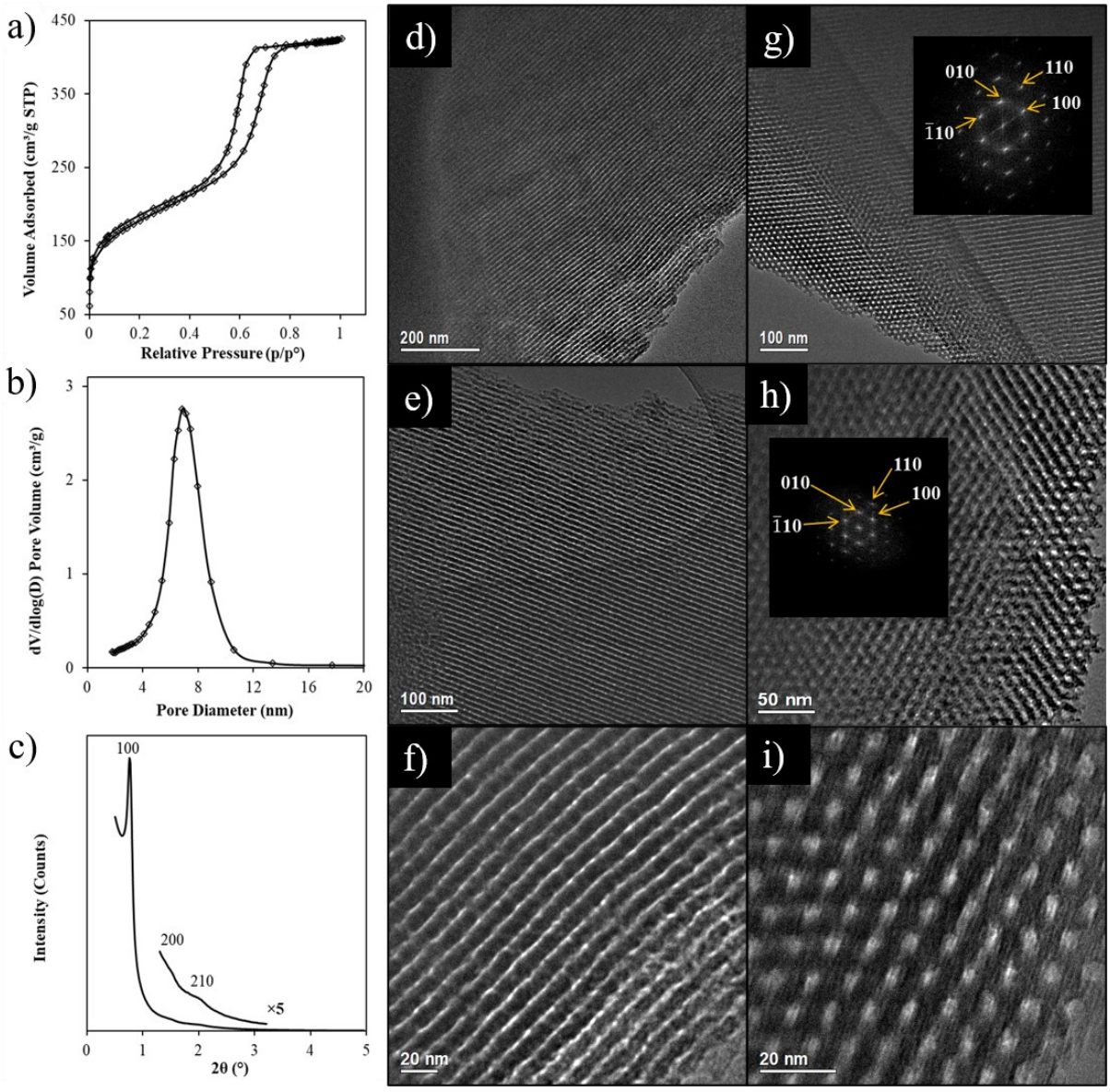

Figure 3. **Scanning Electron Microscope images of (a) as-prepared OMC and (b) OMC after treatment with MO.**

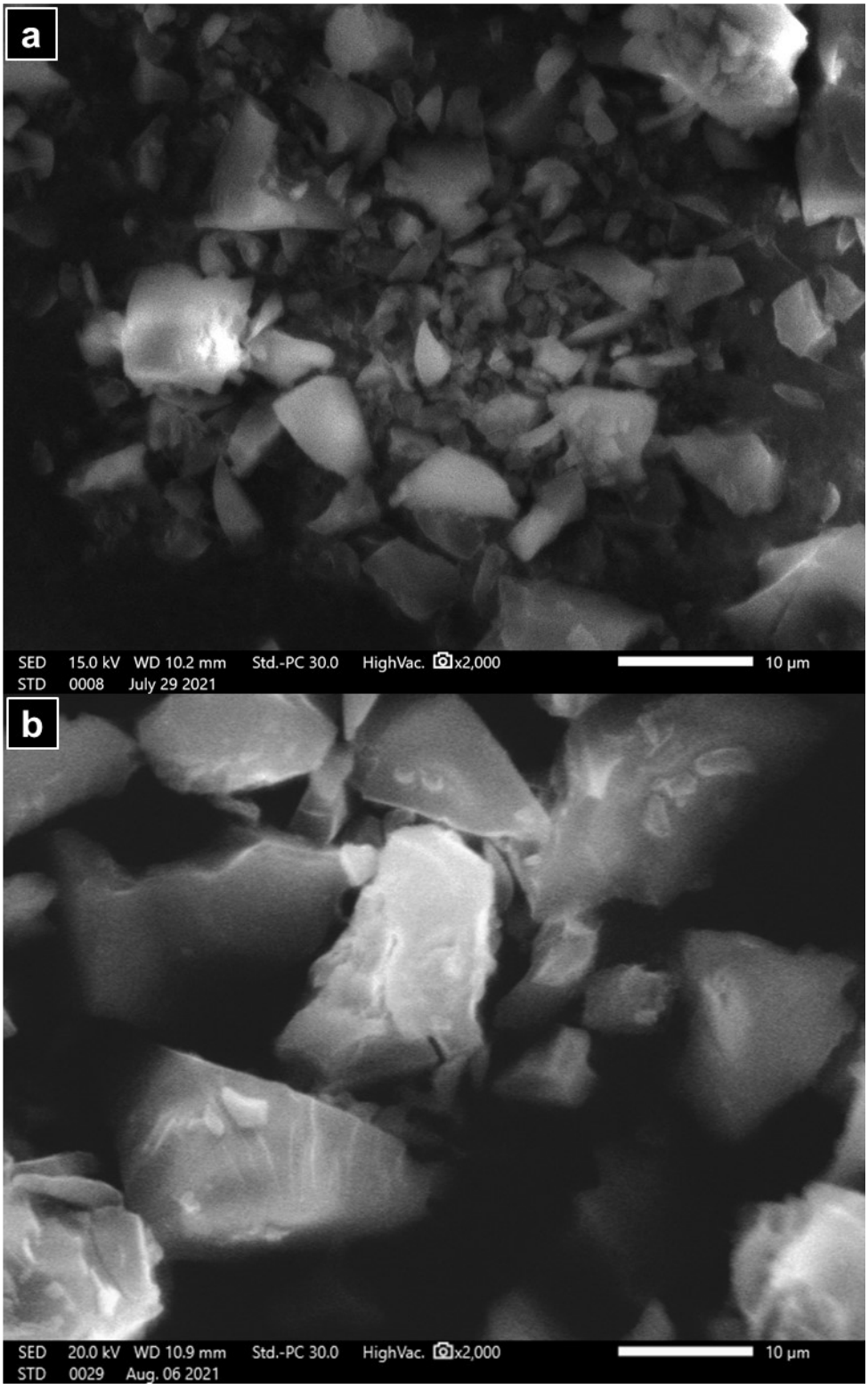

Figure 4. **(a) FTIR spectrum of OMC showing main peak assignments (ar=aromatic, str=stretch); (b) Comparison of FTIR spectra of OMC, MO and OMC treated with MO solution; (c) Solid state ^{13}C MAS NMR spectrum of OMC with main resonances indexed to the representative resol chemical structure (inset).**

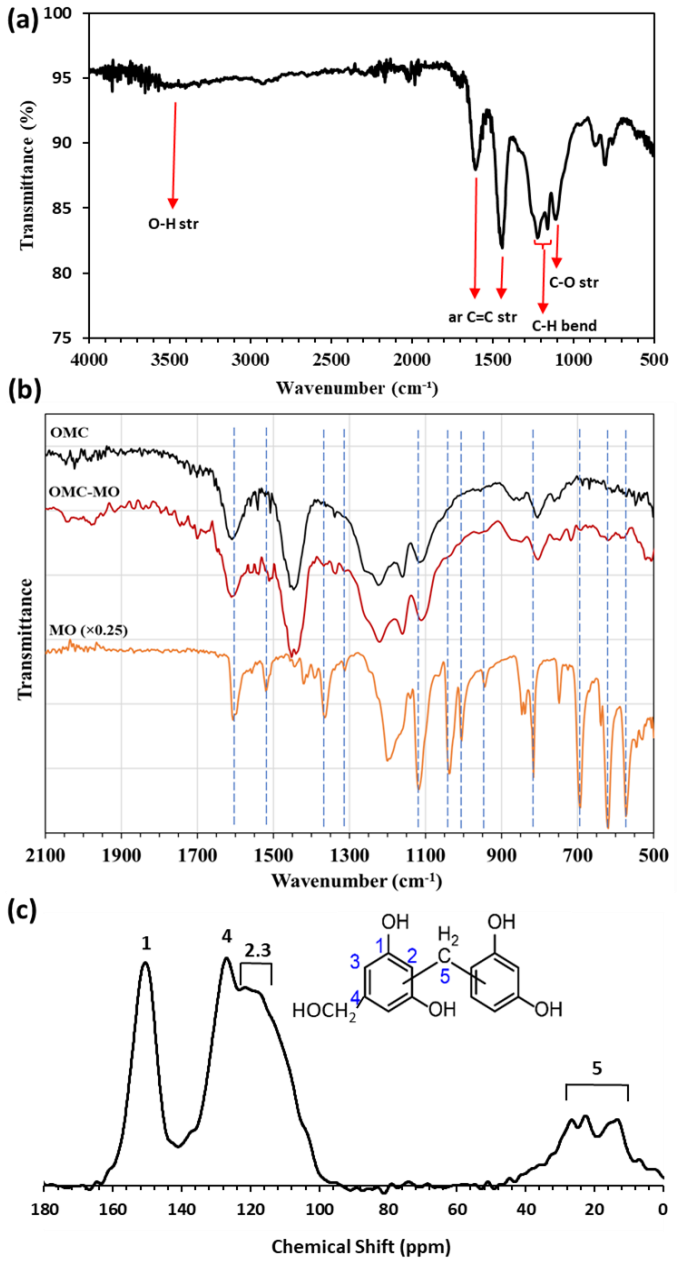

Figure 5. **Effect of pH on the Adsorption of MO over OMC at 303 K (Dye Concentration = 5×10^{-5} M, Adsorbent Dose = 20 mg/20 ml)**

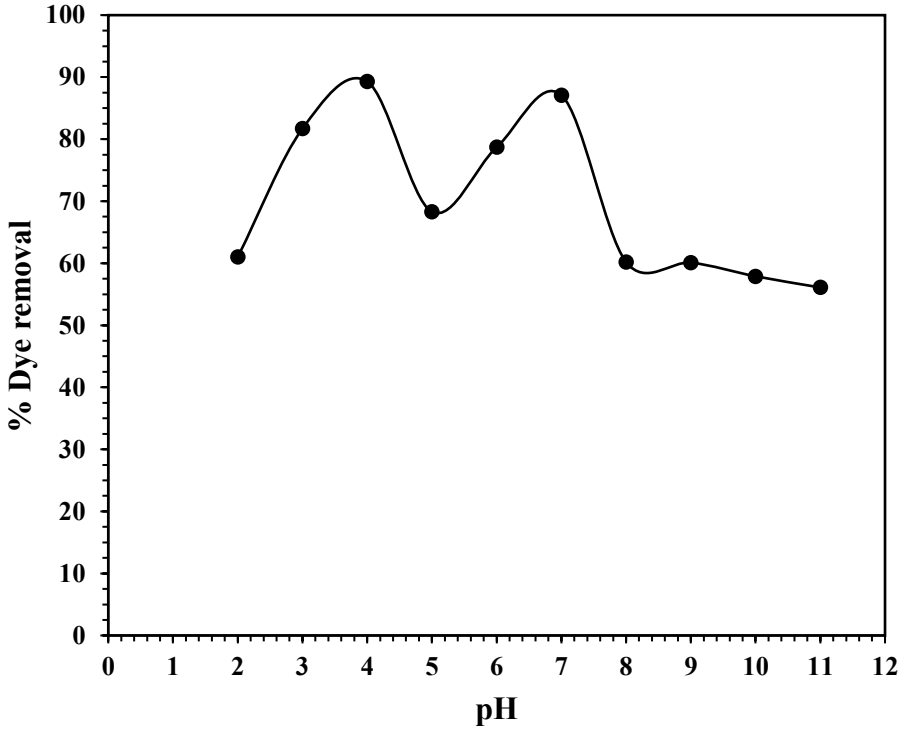

Figure 6. **Effect of the dosage of OMC on the Uptake of MO at 303 K (Dye Concentration = 5×10^{-5} M, pH = 4.0)**

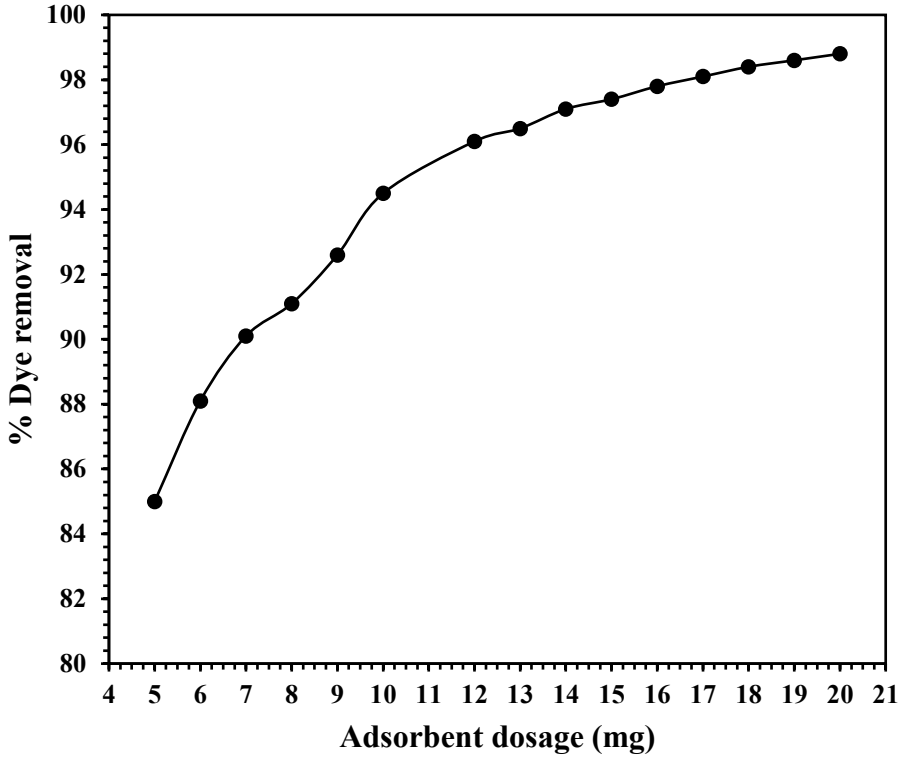

Figure 7. **Effect of Initial Concentration of MO on Adsorption over OMC at 303 K (pH = 4.0, Adsorbent Dose = 20 mg/20 ml)**

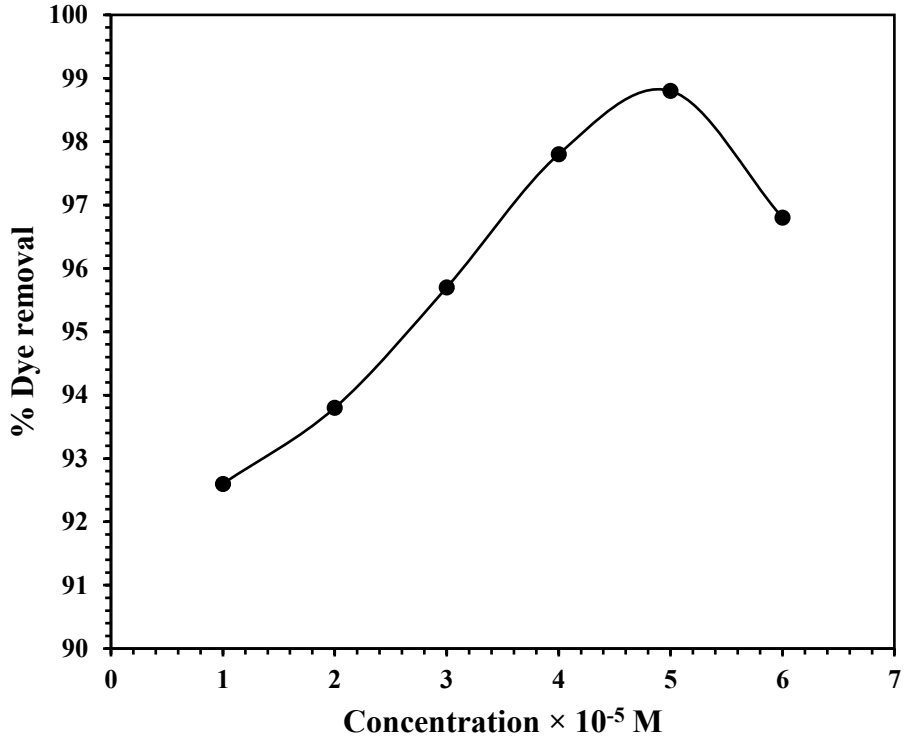

Figure 8. **Effect of Contact Time on the Uptake of MO by OMC at 303 K (Dye Concentration = 5×10^{-5} M, pH = 4.0, Adsorbent Dose = 20 mg/20 ml)**

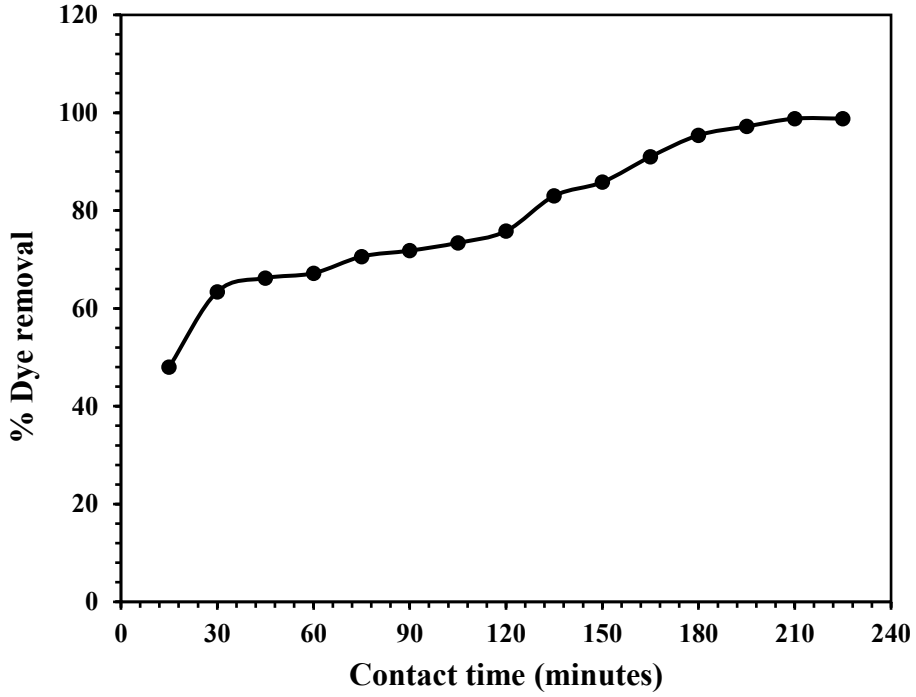

Figure 9. **Plot of t/q_t versus Time for MO (pH = 4.0) – OMC (Dosage = 20 mg/20 ml) System at Different Temperatures**

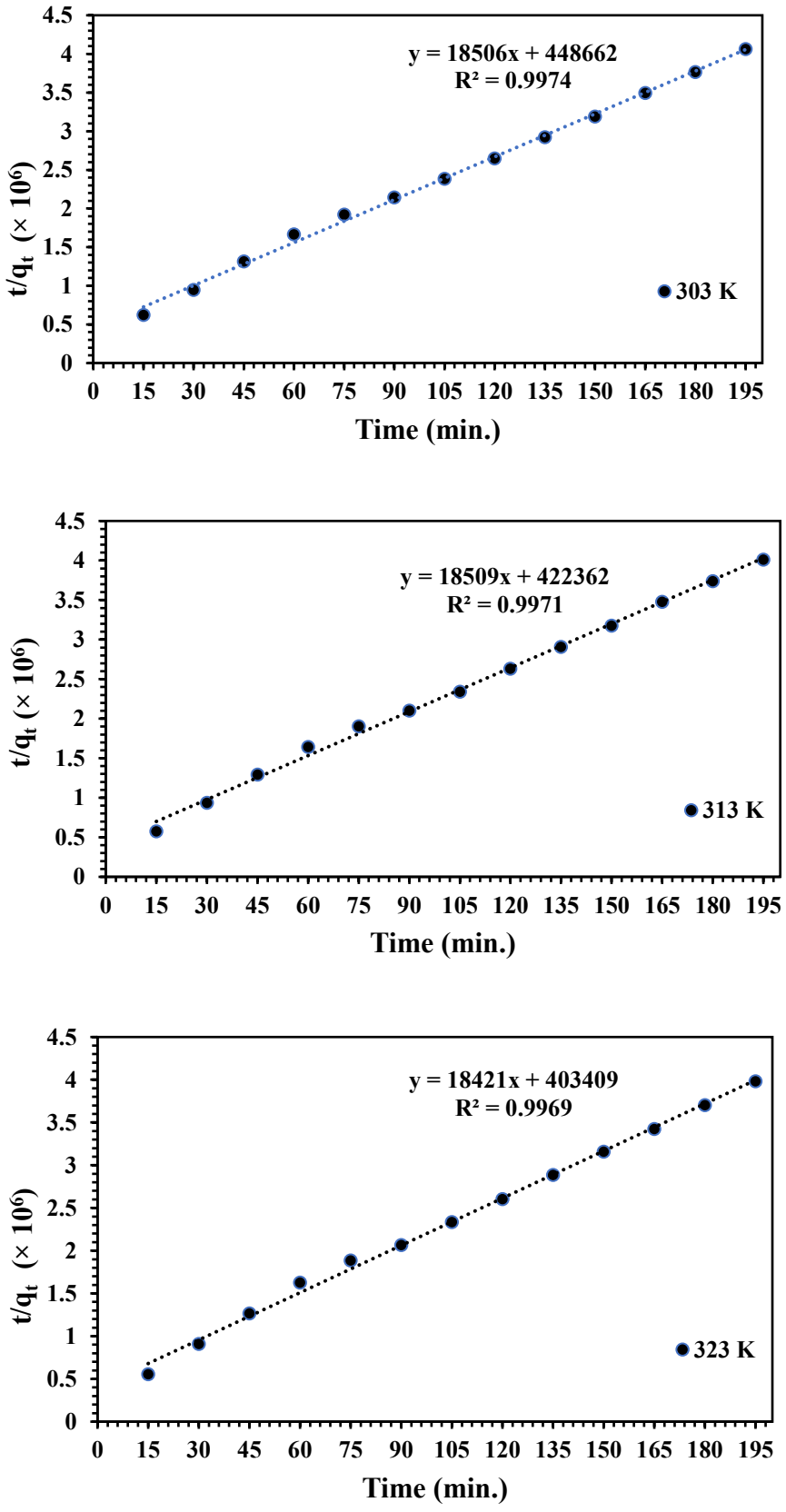

Figure 10. **Plot of B_t versus Time for MO (pH = 4.0) OMC (Dosage = 20 mg/20 ml) System at Different Temperatures**

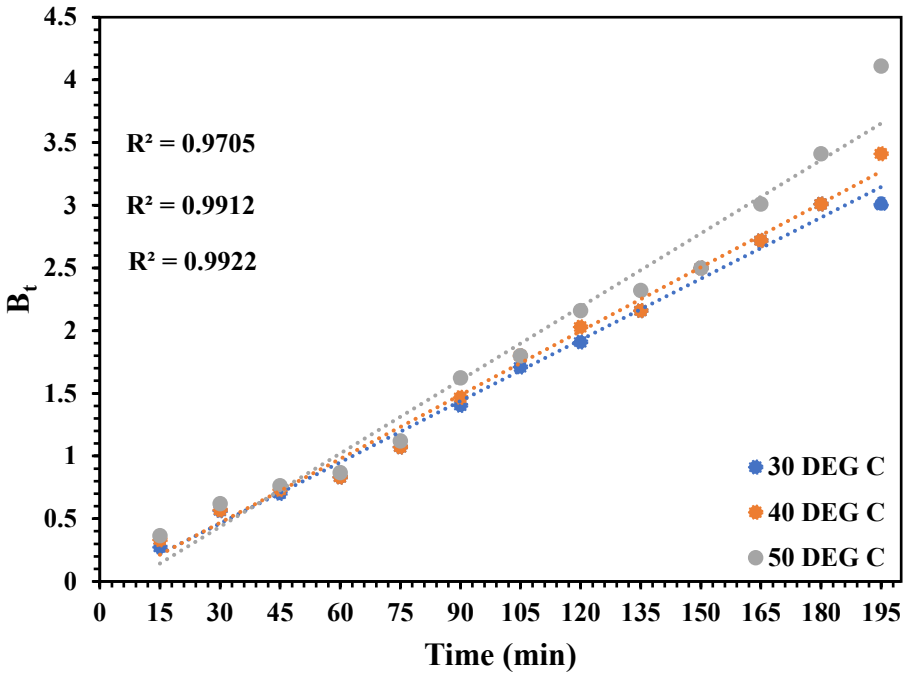

Figure 11. **Plot of ln D_i versus T^{-1} for MO (pH = 4.0, concentration- 5×10^{-5} M) OMC (Dosage = 20 mg/20 ml)**

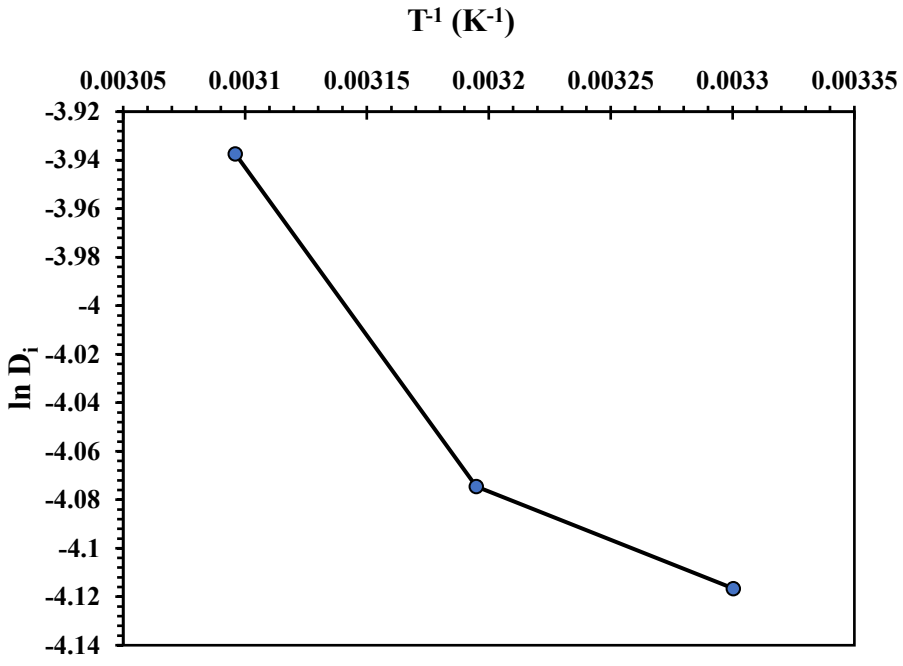

Figure 12. **Plot of log(1-F) versus Time for MO (pH = 4.0, concentration-5 × 10^{-5} M) OMC (Dosage = 20 mg/20 ml)**

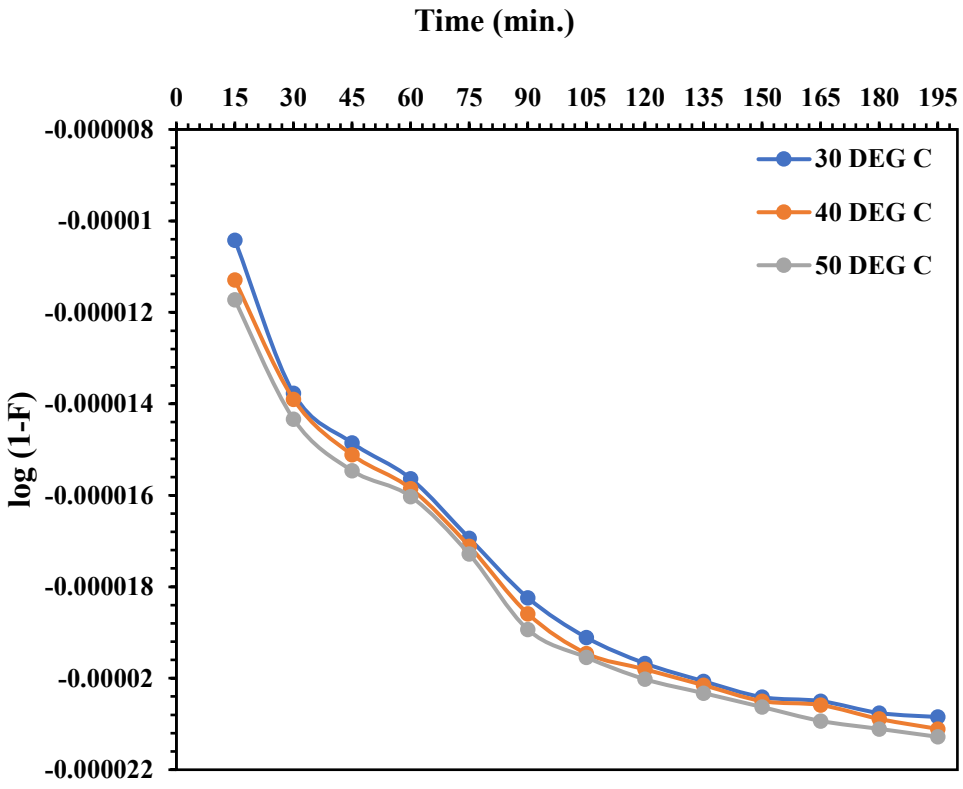

Figure 13. **Plot of q_t versus $t^{0.5}$ for MO (pH = 4.0) – OMC (Dosage = 20 mg/20 ml) System at Different Temperatures**

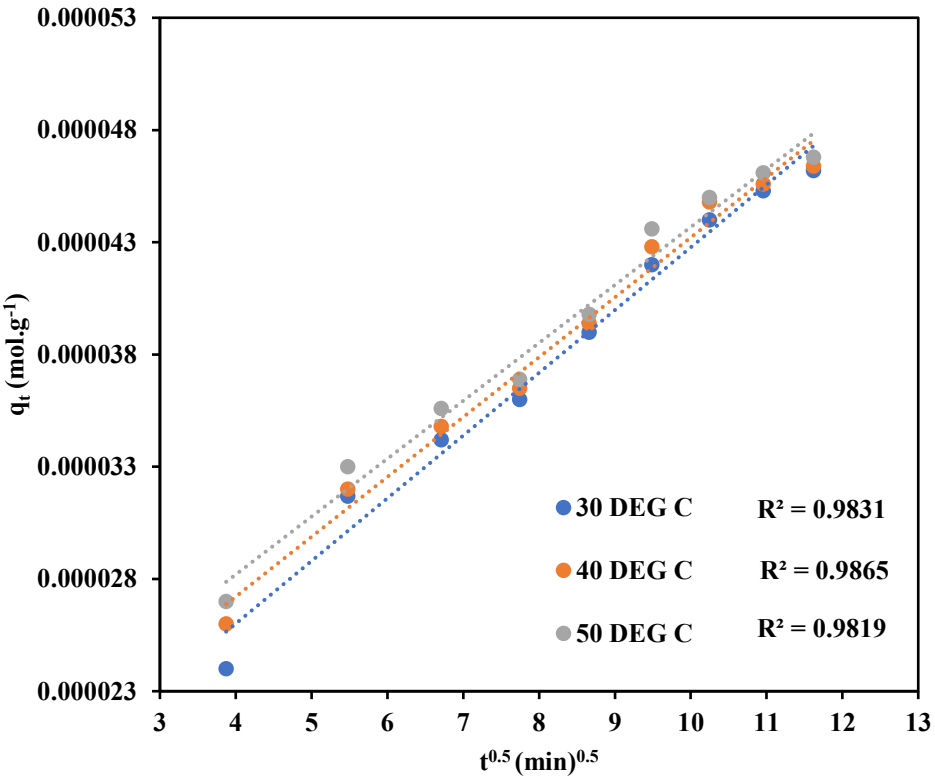

Figure 14. **Langmuir Adsorption Isotherm for MO (pH = 4.0) – OMC (20mg/20ml) System at Different Temperatures**

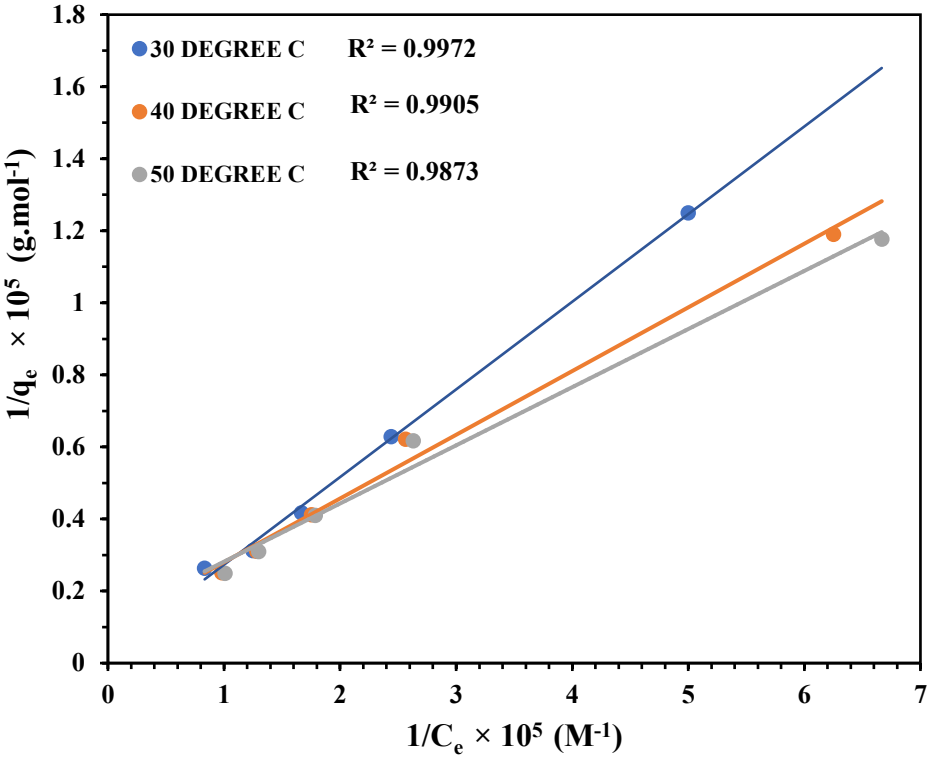

Figure 15. **Freundlich Adsorption Isotherm for MO (pH = 4.0) - OMC (20mg/20ml) System at Different Temperatures**

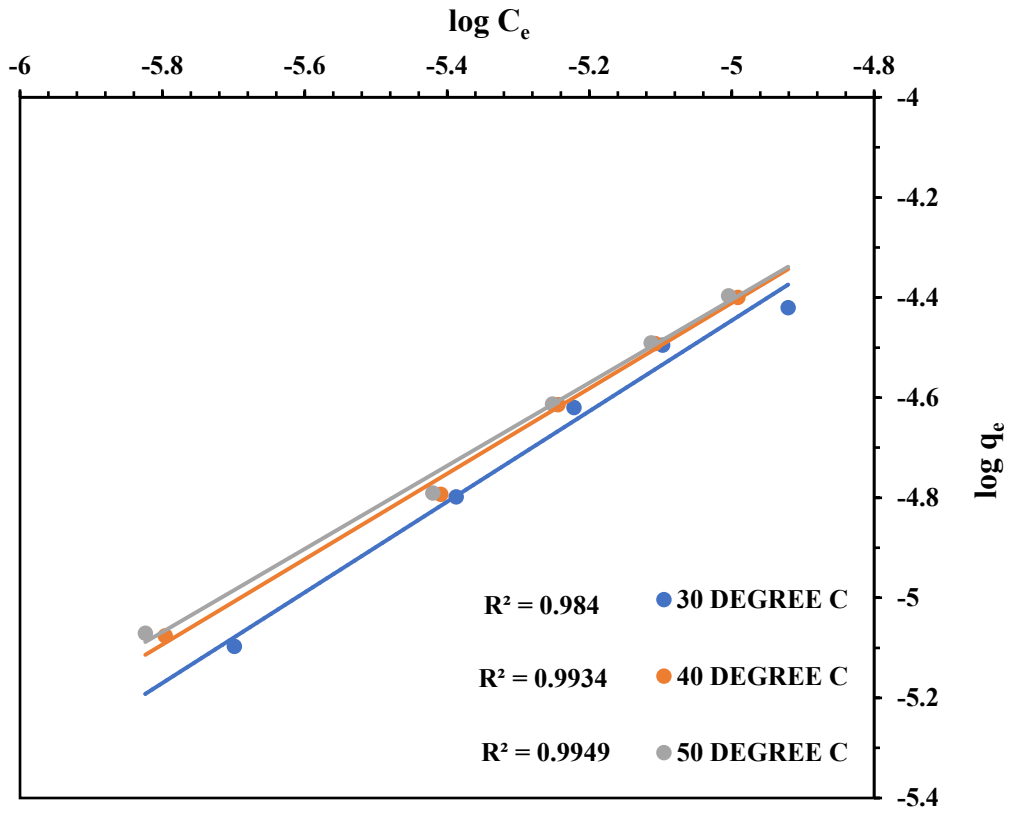

Figure 16. **Temkin Adsorption Isotherm for MO (pH = 4.0) – OMC (20mg/20ml) System at Different Temperatures**

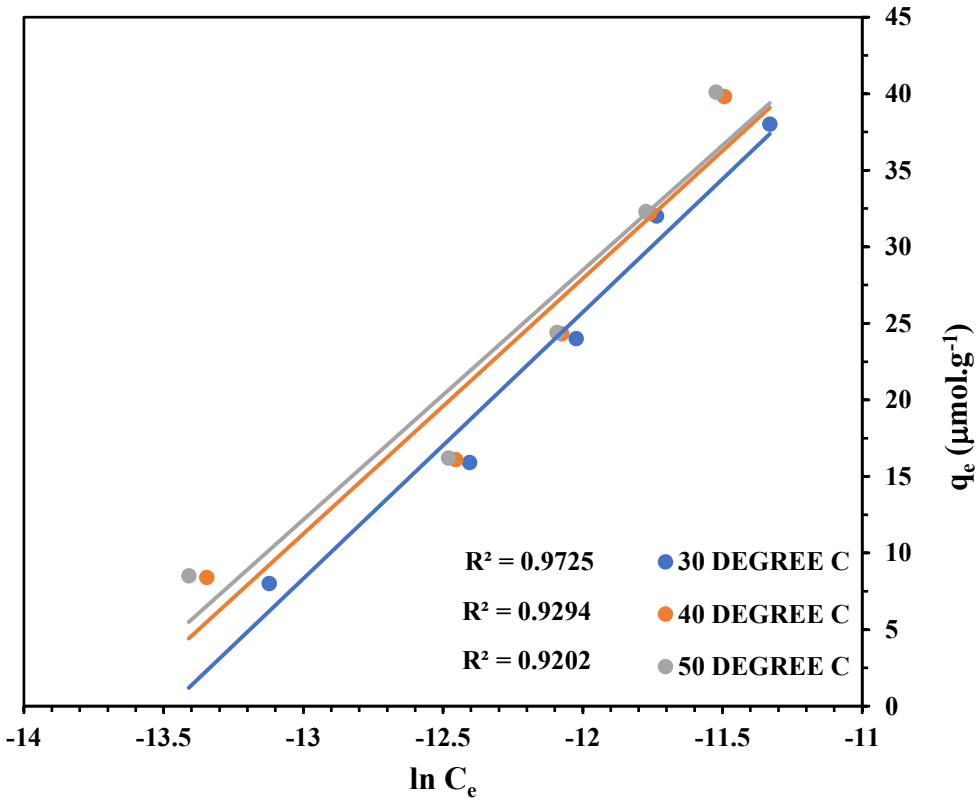

Figure 17. Dubinin-Radushkevitch Adsorption Isotherm for MO (pH = 4.0) – OMC (20mg/20ml) System at Different Temperatures

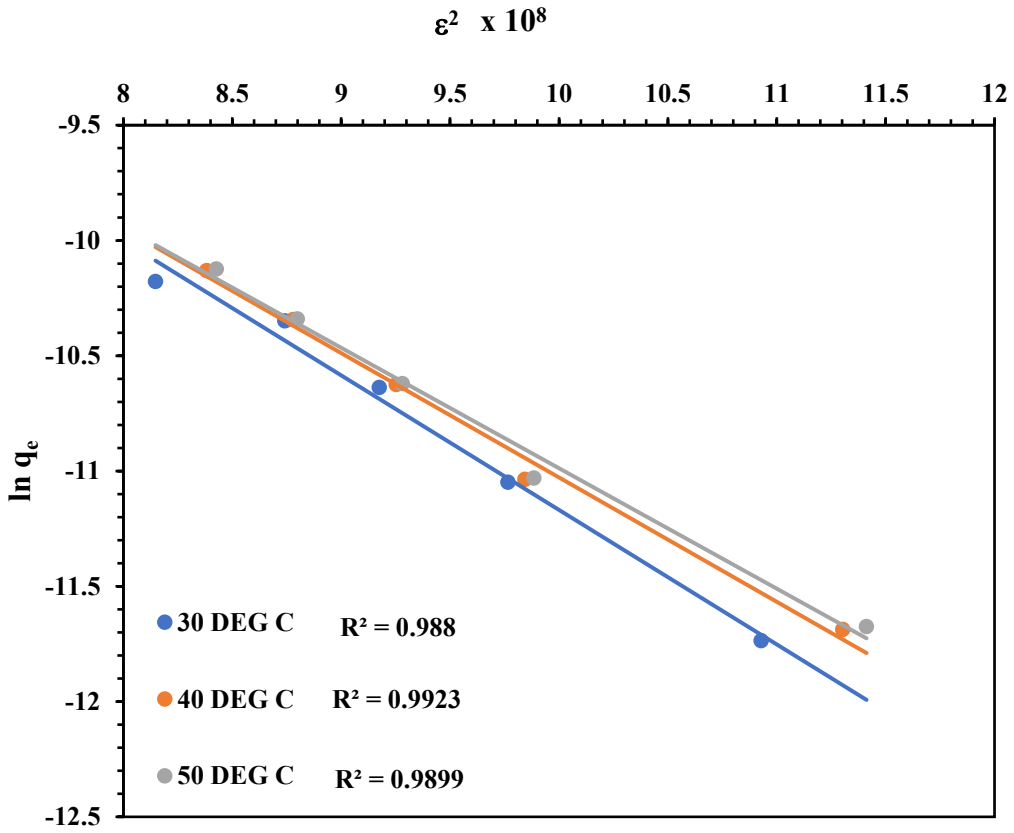

Figure 18. Breakthrough Curve for The Adsorption of MO over OMC in Column Operations (Concentration of feed solution- 1×10^{-3} M, pH- 4.0)

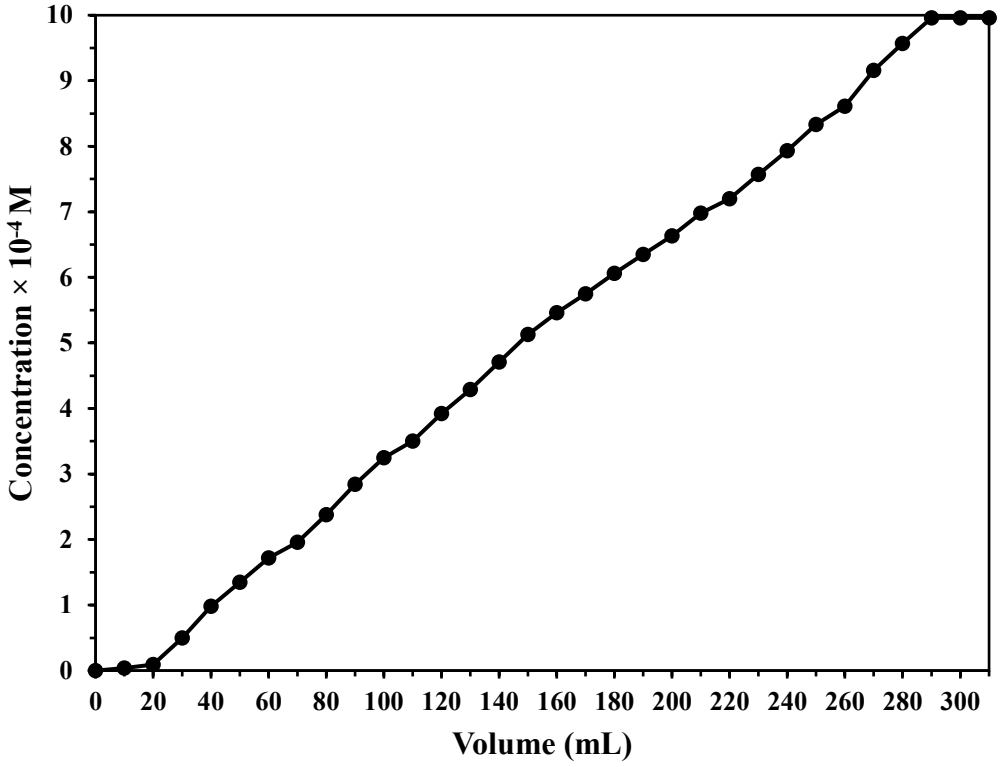

Figure 19. Desorption of MO from Exhausted Column of OMC (Eluent: 2-Methoxy Ethanol)

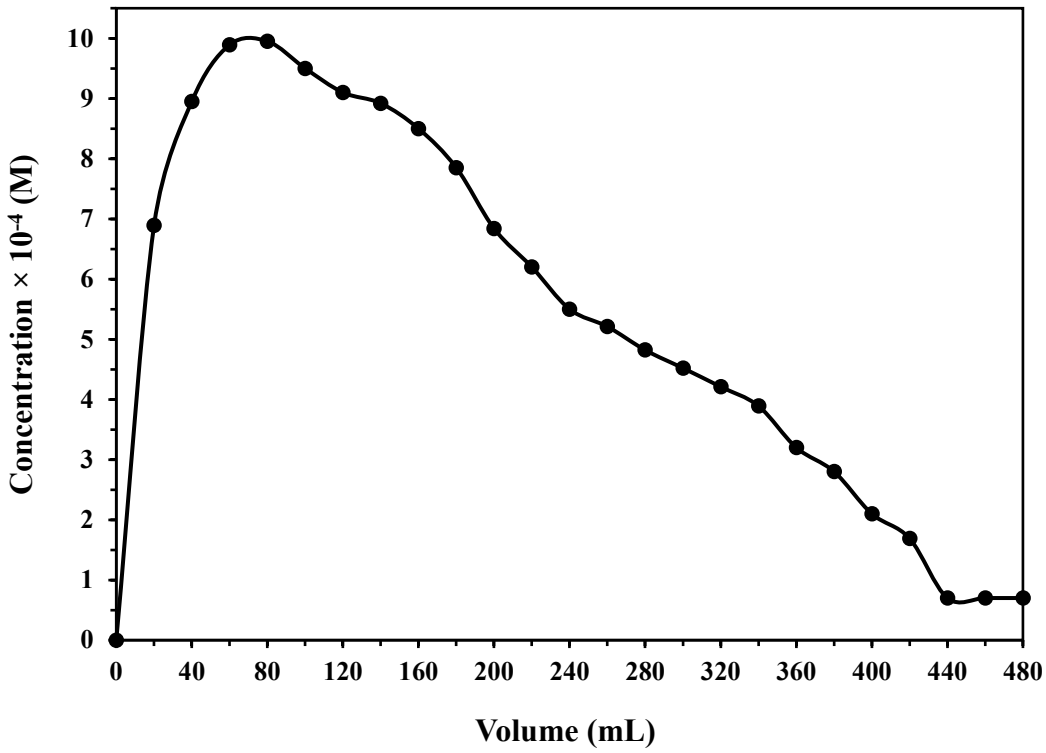

Figure 20. **Plot of Percentage Dye Recovery versus Number of Adsorption-Desorption Cycles**